Bloomfield, V., W. O. Dalton, and K. E. Van Holde. 1967. Frictional coefficients of multisubunit structures, I: Theory. *Biopolymers* 5:135. [See also p. 149.]
Crowther, R. A., and A. Klug. 1975. Structural analysis of macromolecular assemblies by image reconstruction from electron micrographs. *Ann. Rev. Biochem.* 44:161.
Edelstein, S. J., and H. Schachman. 1973. Measurement of partial specific volume by sedimentation equilibrium in H_2O–D_2O solutions. In *Methods in Enzymology*, vol. 27, ed. L. Grossman and K. Moldave (New York: Academic Press), p. 83.
Eisenberg, H. 1976. *Biological Macromolecules and Polyelectrolytes in Solution*. Oxford: Claredon Press. [A useful advanced treatise.]
Fujita, H. 1975. *Foundations of Ultracentrifuge Analysis*. New York: Wiley.
Kratky, O., H. Leopold, and H. Stabinger. 1973. The determination of the partial specific volume by a mechanical oscillator technique. In *Methods in Enzymology*, vol. 27, ed. L. Grossman and K. Moldave (New York: Academic Press), p. 98.
Van Holde, K. E. 1971. *Physical Biochemistry*. Englewood Cliffs, N.J.: Prentice-Hall.

Optional (Cantor & Schimmel)

Set 2-5

11
Ultracentrifugation

11-1 VELOCITY SEDIMENTATION

Any external force acting on suspended particles can lead to mass transport (as described in Eqn. 10-37). Different types of forces require rather different types of experimental apparatus and involve rather different aspects of molecular structure and properties. In this chapter we treat (in considerable detail) the transport resulting from the response to a particular force: radial acceleration in an ultracentrifuge. This example is chosen because, in practice, ultracentrifugation is by far the most widely used hydrodynamic technique for precise analysis of macromolecular properties.

Sedimentation by gravity or by angular acceleration

Gravitational force has an appealing feature for the determination of particle mass: all particles feel it. The force depends only on the mass and not on charge, shape, or details of chemical composition. Unfortunately, the earth's gravity is very weak, and only the largest subcellular biological structures (such as entire metaphase chromosomes) are really affected by it strongly enough to settle from an aqueous solution. Classical gravity-induced sedimentation is used in the analysis of sizes of large particles (such as sand) and can even be used to separate living cells by size or density.

If an initially homogeneous suspension of uniform large particles is allowed to stand undisturbed, the particles will settle to the bottom of their container, providing

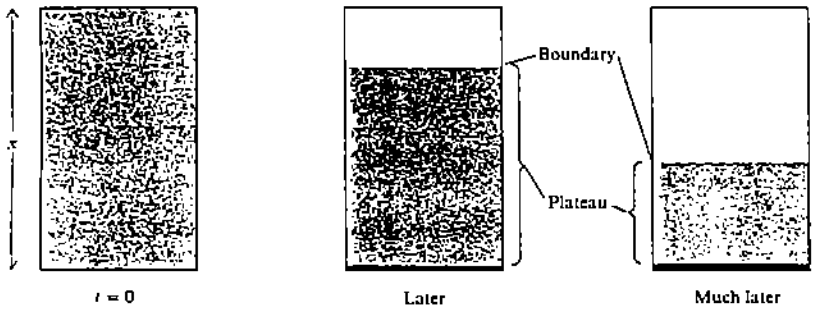

Figure 11-1

Sand settling in a container under the influence of gravity. The initial aqueous suspension is assumed to be uniform. As time proceeds, note the occurrence of a sharp boundary, above which there is only water, and below which there is sand at the same uniform concentration as the original suspension. A second sharp boundary marks the upper limit of the solid sand that has settled out at the bottom.

that they are more dense than the solution (Fig. 11-1). The important thing to note is that a boundary forms as the particles settle. Above this boundary is pure solvent. Below it is a suspension at the same weight concentration as the original homogeneous mixture. This occurs because all particles feel the same gravitational force and therefore move (on the average) with the same velocity. Thus the boundary moves with the same velocity as that of the average sedimenting particle. Note that, if the particles are less dense than the solvent, they will rise rather than sink—just as cream eventually floats out on the top of whole milk.

Now ponder this question: Why do large particles (denser than water) sediment, whereas dense small particles do not? As we shall show, the rate of sedimentation of a particle increases with increased molecular weight, but the rate of diffusion decreases with increased molecular weight. In the limit of large particles such as sand grains, sedimentation is completely dominant and occurs with a very sharp boundary. In the limit of very small particles, diffusion is almost completely dominant, and no boundary forms. However, there is still at least a slight tendency for any particles more dense than the solvent to be found near the bottom of a container rather than near the top. We shall calculate this probability later.

Forces much larger than the earth's gravity are required to cause appreciable sedimentation of typical proteins or nucleic acids. Such forces can be obtained by subjecting particles to an accelerating field. The force is just $F = ma$ for linear acceleration, but it is impractical to sustain such accelerations for extended time periods. The logical alternative is angular acceleration. The radial force produced in a spinning object of mass m is

$$F = m\omega^2 r \qquad (11\text{-}1)$$

where r is the radius from the center of rotation, and ω is the angular frequency in radians per second. For a mass of 1 g, rotation at 60,000 rpm produces a force of 3.95×10^8 dyn at a radius of 10 cm. This is more than 400,000 times the force of gravity (which is 980 dyn at the earth's surface). Such a force may seem very strong, but it is not sufficient to render diffusion forces insignificant for most proteins or nucleic acids. Thus, the simultaneous effects of sedimentation and diffusion must be considered when we describe motion of macromolecules in the ultracentrifuge.

The ultracentrifuge

Considerable ingenuity has gone into the design of ultracentrifuges, instruments that can spin a sample of solution at up to 70,000 rpm. Figure 11-2 is a schematic diagram of an analytical ultracentrifuge. Samples are held in cells or tubes (Fig. 11-3) in an

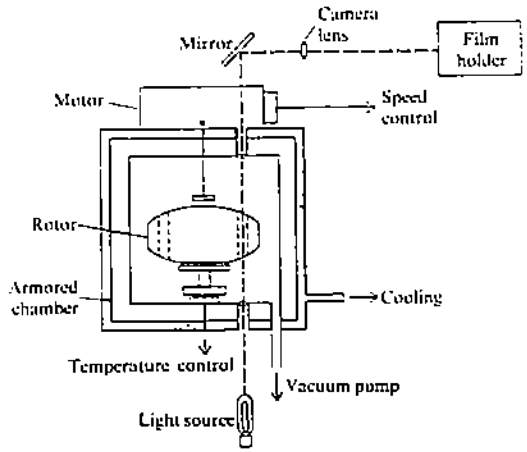

Figure 11-2

Schematic of a modern analytical ultracentrifuge. [After D. Freifelder, *Physical Biochemistry*, p. 270. (San Francisco: W. H. Freeman and Company.) Copyright © 1976.]

aluminum or titanium rotor driven by an electric motor. At typical rotor speeds, friction between the spinning rotor and air would cause intolerable heating. Thus, the chamber in which the rotor spins must be brought to a high vacuum. The temperature of the sample must be regulated precisely, to avoid convective mixing, and this regulation can be difficult. The forces generated within the rotor are enormous, and it is not all that uncommon for a rotor to fly into fragments at high speeds. Thick steel guard rings must surround the rotor chamber to contain these fragments.

Mechanical balance of the rotor is critical. Suppose two sample cells 180° apart on the rotor differ in weight by a milligram. At 400,000 × g, the net force differential on the rotor will be almost a pound. This force is quite considerable and would cause the rotor to wobble on its axis. It is important to balance sample weights, but

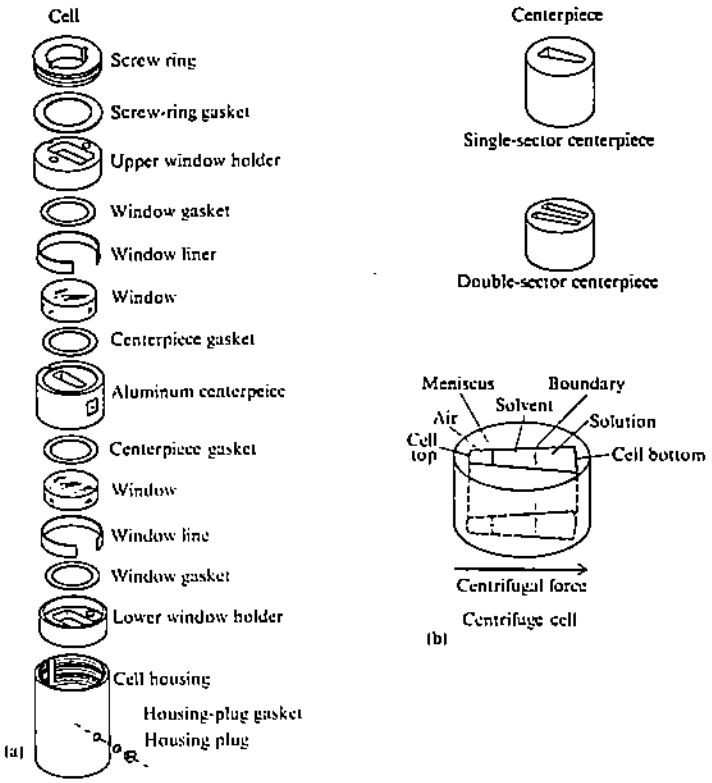

Figure 11-3

Centrifuge cell and centerpieces. (a) Exploded view of the cell. (b) The centerpiece. [Courtesy of Beckman Instruments.]

they cannot be balanced perfectly. Therefore, a flexible shaft is used in any ultracentrifuge so that the rotor can find its precise center of mass in each case and spin about an axis through that center. This allows a sample mismatch of up to 0.5 g in analytical rotors without adverse effects.

There are two basic applications of ultracentrifugation: preparation and analysis. As a preparative technique, it can be used to purify samples or to separate mixtures for subsequent analysis. Here, the sample is spun at high speed in a cylindrical

tube for a fixed time period and then removed from the centrifuge before any measurements are performed. The advantages of this approach are that large sample volumes (5 to 100 ml) can be used, and that a wide variety of biochemical and physical measurements are possible on the recovered sample. The disadvantages are that some stirring or mixing inevitably accompanies slowing the rotor and isolating the sample, and that much information is lost because only a single time point is available.

In analytical ultracentrifugation, the bulk movement of solute molecules is monitored directly as a small sample (0.1 to 1 ml) is spun in the rotor. This is made possible by optical systems that send light through the sample parallel to the rotation axis. The optical system can be absorbance, Rayleigh interference, or Schlieren—the same three systems mentioned for study of diffusion.

A critical feature of the analytical ultracentrifuge is the design of the sample cell. This cell must be sector-shaped when viewed parallel to the rotation axis (Fig. 11-3b). Because the acceleration force is radial, sedimenting molecules will move along radii. If a rectangular cell were used (Fig. 11-4a), the paths of many molecules would lead to collision with the side walls of the cell. They might remain there, or

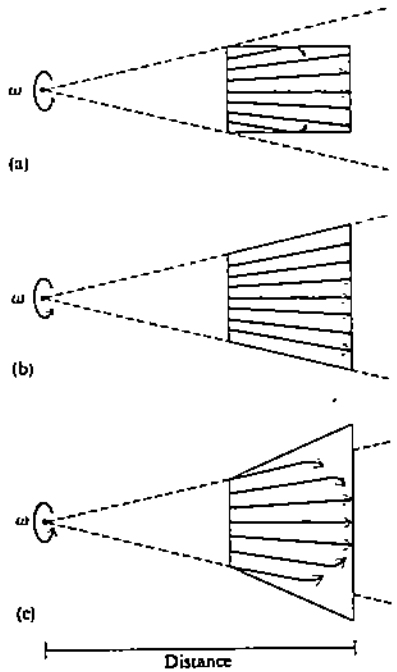

Figure 11-4

Expected solute transport in ultracentrifuge cells of different geometries. In each case, the cells are viewed looking down the axis of rotation. (a) In a rectangular cell, the solute collides with the walls. This cell is equivalent to the cylindrical tubes used in all preparative ultracentrifuges. (b) In the sector-shaped cell used in all analytical ultracentrifuges, the solute moves freely along radial paths. (c) In a cell diverging more sharply than a sector, the solvent collides with the walls and then deflects the solute from the walls.

they might pile up and ultimately fall to the bottom, causing stirring. In either case, the boundary conditions needed to describe the hydrodynamics become very complicated. One might think that the cell shape in Figure 11-4c would circumvent these problems, but it does not. This is because every solute movement must be accompanied by a compensating solvent flow. If macromolecules are sedimenting from left to right in Figure 11-4, then solvent is moving from right to left. In Figure 11-4c, the water will collide with the walls of the cell and be deflected back toward the center, causing stirring.

The sector shape shown in Figure 11-4b makes quantitative sedimentation measurements possible but, as you will shortly see, seriously complicates the mathematical analysis of the experiment. Sample cells in preparative ultracentrifugation traditionally are cylindrical tubes—definitely not sector-shaped. Therefore, some solute molecules are lost on the walls in these tubes—an effect for which correction must be made if accurate quantitation of the results is desired. In practice, not all investigators remember to make the necessary corrections.

Describing transport in the ultracentrifuge: the Lamm equation

Figure 11-5 is an expanded view of a sector-shaped sample cell. Defined are the solvent–air interface, x_m (the meniscus), x_b (the bottom of the cell), ϕ (the angle of the sector shape), and a (the thickness of the cell along the rotation axis). We can treat the hydrodynamics of sedimentation as a one-dimensional problem, with x characterizing the distance from the rotation axis. Because the coordinate x is a radial distance, it defines the location of radial-shaped surfaces.

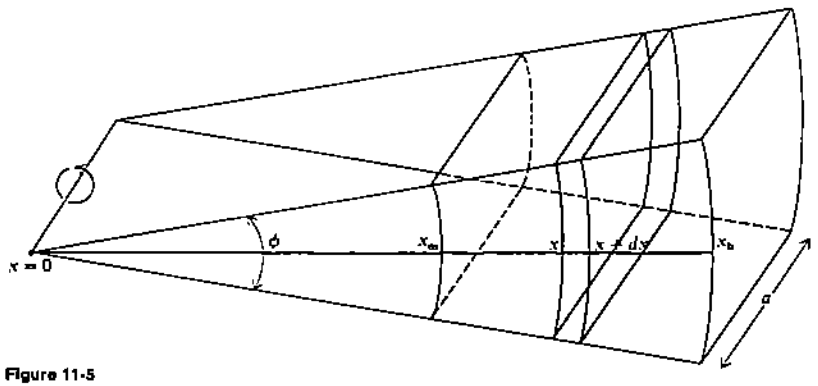

Figure 11-5

Geometry of a typical sector-shaped ultracentrifuge cell. The radial distance is x; the position of the meniscus is x_m (effectively the top of the solution, rather than the actual physical top of the cell); the bottom of the cell is x_b. The rotation axis is at $x = 0$. Mass transport in the zone between x and $x + dx$ is considered in deriving the Lamm equation (Eqn. 11-7).

Consider a system with two components, solvent (1) and solute (2). The phenomenological equation for flux (Eqn. 10-39) immediately yields an equation for the rate of solute mass transport across a surface at radius x in the ultracentrifuge:

$$J_2 = L_{22}[\omega^2 x - (\partial\bar{\mu}_2/\partial x)] \tag{11-2}$$

The first term within brackets accounts for the force due to radial acceleration per gram of macromolecules; the second term describes the diffusion force that will develop in the presence of any chemical potential gradients.

First, we shall use a mechanical description of the sedimentation experiment to identify experimentally measurable parameters. Then, we shall use the thermodynamics of the experiment to connect measured quantities with molecular parameters. The applied force causing flow in the centrifuge is $\omega^2 x$ per unit mass. If there is no diffusion, this force will produce a constant drift velocity (v) in the hydrodynamic steady state. The velocity will be a function of the size and shape of the sedimenting particle, but it must be proportional to the applied force. We define that proportionality constant (s) to be the sedimentation coefficient:

$$s = v/\omega^2 x = (1/\omega^2 x)(dx/dt) \tag{11-3}$$

From Equation 11-3, the units of s are seconds. However, measurements usually are expressed in Svedberg units ($1\ \mathrm{S} = 10^{-13}$ sec), named after The Svedberg, the inventor of the ultracentrifuge. Keep in mind that s is defined as the velocity per unit field; therefore, any measured value of s should be independent of the angular rotation frequency of the ultracentrifuge.

We can use the definition of s to describe the flux across the surface at radius x in Figure 11-5. Equation 11-2 ensures that contributions due to sedimentation and diffusion can be described separately. If the concentration of solute molecules at x is c_2 g cm^{-3}, and if they all are moving at velocity $v = \omega^2 xs$ due to the applied force, then the flux caused by angular acceleration is $c_2\omega^2 xs$. If there is a concentration gradient at x, then there will be a flux due to diffusion given by Fick's first law (Eqn. 10-45). Thus, Equation 11-2 becomes

$$J_2 = \omega^2 xsc_2 - D(\partial c_2/\partial x) \tag{11-4}$$

We want to calculate the change in solute concentration in a volume element located a distance x from the rotation axis. First consider the total mass transport across the surface at x. Because J_2 is a flux per unit area, the total mass transport is J_2A. The area A of the surface at radius x is $ax\phi$. Just as we did earlier in discussing diffusion, we must develop an equation for the conservation of mass. The total rate of solute mass change in the volume bounded by surfaces at radii x and $x + dx$ will be

$$dm_2/dt = J_2A(x) - J_2A(x + dx) \tag{11-5}$$

The concentration change is the mass change divided by the volume between the two surfaces:

$$\begin{aligned} dc_2/dt &= (1/\phi x a\, dx)[J_2A(x) - J_2A(x + dx)] \\ &= (-1/\phi x a)(dJ_2A/dx) = -(1/x)[d(xJ_2)/dx] \end{aligned} \tag{11-6}$$

Combining Equations 11-4 and 11-6, we obtain the Lamm equation:

$$\boxed{\frac{dc_2}{dt} = \left(\frac{1}{x}\right)\frac{d\{x[D(dc_2/dx) - c_2s\omega^2x]\}}{dx}} \tag{11-7}$$

This is the most general hydrodynamic description of the mass transport of a two-component system in the ultracentrifuge.

At low solute concentration, the diffusion and sedimentation constants should be independent of concentration. Equation 11-7 then can be simplified:

$$\boxed{dc_2/dt = D[(d^2c_2/dx^2) + (1/x)(dc_2/dx)] - s\omega^2[x(dc_2/dx) + 2c_2]} \tag{11-8}$$

A few of the features of this equation are worth noting. If ω^2 is zero, Equation 11-8 simply describes diffusion. It differs from the form of Fick's second law (Eqn. 10-50) because of the sector-shaped cell. Note that the second diffusion term is undefined at $x = 0$. This is not a problem, because one never places the beginning of a cell at the rotation axis. Even if one did, the volume (and therefore the mass) at that point would be zero anyhow.

Solving the Lamm equation with constant s and no diffusion

If D is zero, Equation 11-8 can be solved exactly (see Fujita, 1975). For a sample that at zero time has a uniform solute concentration c_0, the results are

$$\boxed{\begin{aligned} c_2(x, t) &= 0 && \text{if } x_m < x < \bar{x} \\ c_2(x, t) &= c_0e^{-2s\omega^2t} && \text{if } \bar{x} < x < x_b \end{aligned}} \tag{11-9}$$

where

$$\boxed{\bar{x} = x_me^{s\omega^2t}} \tag{11-10}$$

Here we have ignored the accumulation of material at the bottom of the cell.

Figure 11-6a shows these results schematically. There is a sharp increase in solute concentration from zero to a value that is independent of x at any particular time. The

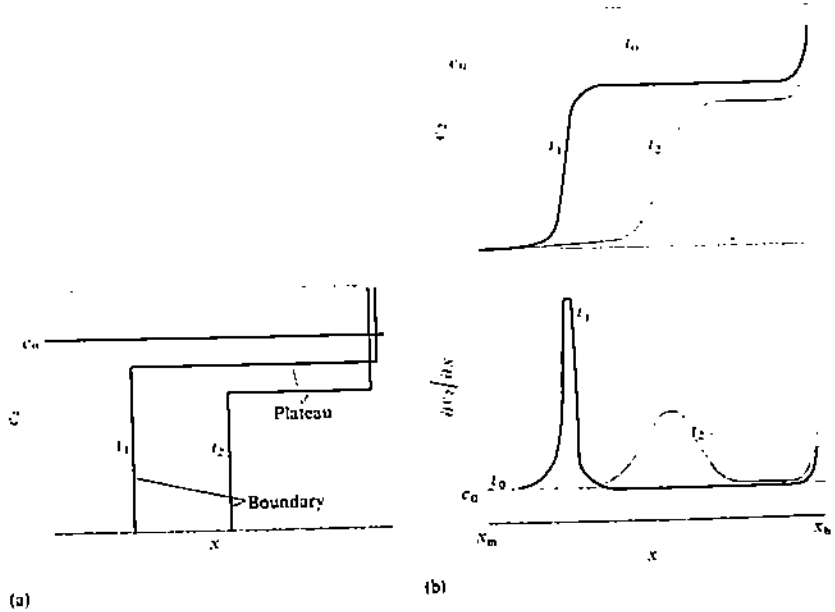

Figure 11-6

Solute concentration profiles during ultracentrifugation of a typical solution of a homogeneous macromolecule. The times shown might be $t_0 = 0$ hr, $t_1 = 1$ hr, and $t_2 = 2$ hr for a large protein at 50,000 rpm. (a) If $D = 0$, a sharp boundary is formed. The boundary moves in time. Above the boundary is a flat plateau, whose concentration decreases with time. (b) If $D \neq 0$, diffusion causes a broadening of the boundary as a function of time. The concentration gradient ($\partial c_2/\partial x$) is also shown, as it might be measured by some optical systems used in the ultracentrifuge.

step-function increase occurs at $\bar{x}$, which is called the boundary position. The position $\bar{x}$ changes with time, moving with increasing speed (as shown by Eqn. 11-10). The region $x > \bar{x}$ is called the plateau. It remains "flat" (uniform concentration), but the actual concentration decreases progressively with time (as shown by Eqn. 11-9).

It may seem paradoxical that a region of x-independent solute concentration can be maintained in the cell while the concentration in this region decreases exponentially with time. This occurs because the radial acceleration and the cross-sectional area both increase linearly with x, and their effects are combined. Consider a thin layer of solution at position $x' > \bar{x}$ at time t_1. There molecules are sedimenting with velocity $v' = \omega^2 s x'$. Pick another layer at position $x'' > x'$ (Fig. 11-7). Molecules there

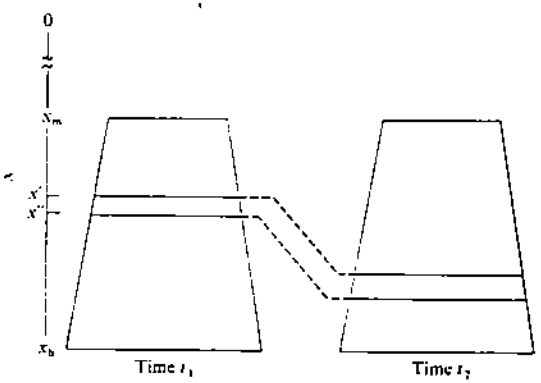

Figure 11-7

Demonstration of radial dilution. A finite zone of solute is followed from an early to a late time during velocity sedimentation. Each dot represents a single macromolecule. The area of the solute zone increases because of the sector shape. Furthermore, the zone thickness increases slightly because the solute at the bottom (x'') is always subjected to a somewhat larger acceleration ($\omega^2 x''$) than is the solute at the top (x'), which feels an acceleration of $\omega^2 x'$, so that the bottom of the zone accelerates away from the top of the zone.

are moving at velocity $v'' = \omega^2 s x'' > v'$. The two layers define a zone as shown in the figure. Now examine the position of the two edges of the zone at some time t_2. The molecules originally at x'' have moved farther than those originally at x', because they have been subjected to stronger radial acceleration at all times. Therefore, the width of the zone increases with time. The area of the zone also increases because of the sector shape. Thus the concentration of solute in the zone drops (because the number of solute molecules inside has remained constant while the volume has increased). This effect is called radial dilution.

To show that a plateau is maintained, we must demonstrate that all zones are subject to the same radial dilution. It is sufficient to prove that the relative volume

change of a zone is independent of its position. The volume V of a zone is its thickness $(x'' - x')$ multiplied by its area. The area is the average of the two surfaces: $\frac{1}{2}(\phi x' a + \phi x'' a)$. Therefore,

$$V = \tfrac{1}{2}\phi a[(x'')^2 - (x')^2] \tag{11-11}$$

The velocity of the x' surface of the zone is

$$v' = dx'/dt = \omega^2 s x' \tag{11-12}$$

For a surface originally (time t_1) located at $x'(t_1)$, solution of this simple differential equation gives, at time t_2,

$$x'(t_2) = x'(t_1)e^{\omega^2 s(t_2 - t_1)} \tag{11-13}$$

Similarly, for a surface originally located at $x''(t_1)$, we obtain

$$x''(t_2) = x''(t_1)e^{\omega^2 s(t_2 - t_1)} \tag{11-14}$$

Thus the volume of the zone at time t_2 compared with that at time t_1 is

$$\begin{aligned} V(t_2)/V(t_1) &= \tfrac{1}{2}[[x''(t_2)]^2 - [x'(t_2)]^2]/\tfrac{1}{2}[[x''(t_1)]^2 - [x'(t_1)]^2] \\ &= e^{2\omega^2 s(t_2 - t_1)} \end{aligned} \tag{11-15}$$

This volume ratio is independent of x. Therefore, because the number of molecules in each zone remains constant and each zone increases in volume by the same ratio, the concentrations in all the zones must remain equal. Note that we have, in effect, rederived Equations 11-9 and 11-10. Let $t_1 = 0$ in Equations 11-13 and 11-15, and let $x'(0)$ be the top of the cell (x_m). Then Equation 11-13 is identical to Equation 11-10. If the original concentration at $t = 0$ is c_0, then Equation 11-15 shows that the plateau concentration at a later time t_2 will be diluted to $c_0/e^{2\omega^2 s t_2}$, which is identical to Equation 11-9.

Solving the Lamm equation for more realistic cases

The Lamm equation has been solved analytically or numerically only in certain limiting cases (Box 11-1). The results show that there is in fact a boundary and a plateau, so long as sedimentation forces are strong compared with diffusion. In these more realistic cases, the boundary is not perfectly sharp, but it has a breadth that is dependent on D. The plateau concentration does decrease with time (Fig. 11-6b). Note that diffusion forces will be felt only near the boundary where there is a concentration gradient. Thus it is reasonable that a plateau can be maintained, even in the presence of diffusion.

Because we now know that a plateau will exist (assuming that s is constant), we can solve Equation 11-8 at the plateau in a very simple fashion. The solute concentration at the plateau (c_p) is not a function of x. Therefore, both dc_p/dx and d^2c_p/dx^2 are zero at all times, and Equation 11-8 becomes

$$dc_p/dt = -2c_p s\omega^2 \tag{11-16}$$

The solution of this differential equation is trivial, using the boundary condition that the concentration of macromolecules at zero time (c_0) is uniform everywhere in the cell:

$$c_p(t) = c_0 e^{-2s\omega^2 t} \tag{11-17}$$

This result is identical to Equation 11-9. Thus, diffusion does not affect the rate at which the concentration of the plateau decreases with time.

Using Equation 11-17, we can compute the sedimentation constant s from a plot of ln c_p versus t. However, direct concentration measurements in the ultracentrifuge are not always easy. For example, Schlieren optics yield $\partial c_2/\partial x$ rather than c_2. An alternative method for determination of s is based on Equation 11-3, which can be rewritten as $s = \omega^{-2}[d(\ln x)/dt]$. If one could observe an individual particle in the plateau region, a plot of the logarithm of its position as a function of time would yield s. Alternatively, if diffusion is negligible, the boundary between solvent and

›x 11-1 SOLUTIONS OF THE LAMM EQUATION

. Fujita (1975) summarizes many of the attempts to solve the Lamm equation. W. J. Archibald ovided (in 1938) an exact analytical solution for Equation 11-8 with s and D constant. owever, the coefficients are so complex that even numerical calculations using the Archibald lutions are too laborious to be of general use in evaluating the results of sedimentation periments.

H. Faxén (in 1929) showed that it is possible to solve Equation 11-8 in a much simpler rm, using special boundary conditions. Instead of the usual sector-shaped cell, he considered ı infinite sector: $x_m = 0$, and $x_b = \infty$. His solution can be adapted to predict the results of dimentation experiments in the limiting case of early times ($\omega^2 st \ll 1$) and weak diffusion $D/s\omega^2 x \ll 1$). The results are essentially identical to those shown in Figure 11-6b. Fujita ı 1956) was able to extend Faxén's solution to cover the case where D is constant, but s ıries with concentration as $s = s_0(1 - k_s c)$.

However, all these solutions are so cumbersome to use that experimentalists usually ıve chosen to adapt simple approaches that permit s to be measured from concentration ıta in only limited regions of the cell. This approach is described in detail in the text.

solution is perfectly sharp, and the velocity of this boundary is the same as the velocity of particles in the plateau. From Equation 11-10, this velocity is $d\bar{x}/dt = s\omega^2\bar{x}$, allowing s to be evaluated as

$$\boxed{s = \omega^{-2}[d(\ln \bar{x})/dt]} \tag{11-18}$$

In a real case, the finite width of the boundary means that molecules at different positions are moving at different net velocities. It is not immediately obvious which position on the boundary to pick to correspond to the motion of the molecules unaffected by diffusion. A common choice is the point of steepest slope, corresponding to a maximal value of $\partial c_2/\partial x$. This choice is made because the point can be measured conveniently; however, it is not a correct choice (although often it leads to only a negligible error).

Obtaining the sedimentation coefficient from the boundary position

We need to find the position on the boundary that moves with the same velocity as that of $\bar{x}$. We can then use this point in Equation 11-18 to compute s. Figure 11-8 shows schematically how the point is located. Suppose we pick some point x_p on the

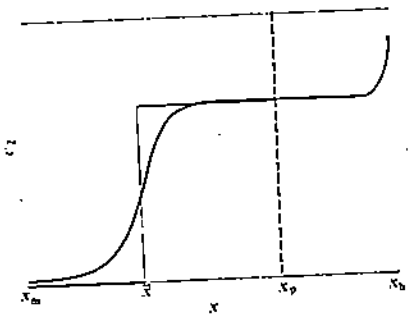

Figure 11-8

Effect of diffusion on sedimentation profile. The sedimentation profile of a real solute (*solid line*) is compared with that expected for a sample of identical sedimentation velocity but no diffusion (*colored line*). A position $\bar{x}$ on the real boundary can be found to move with the same velocity as that of molecules in the plateau region. A position x_p well within the plateau region can be used to measure plateau concentrations, even with the real boundary.

plateau. The total mass m_T of solute between x_m and x_p will decrease as a function of time, as the boundary moves. If m_T is measured, it will reveal how much solute has sedimented past x_p. This amount is unaffected by diffusion or by the shape of the boundary because x_p is in the plateau; m_T depends only on s, ω^2, t, and c_0.

But $\bar{x}$ is the boundary position defined in a hypothetical experiment in which there is no diffusion. To make this experiment correspond to a real experiment (in which the solute has the same value of s), we must ensure that m_T is the same in both

cases. The value of $\bar{x}$ that leads to this result is equal to the boundary position in the real experiment that must be used to calculate s.

We find m_T by integrating the concentration $c_2(x, t)$ multiplied by volume $\phi x a\, dx$. Because the concentration is a simple step function in the hypothetical experiment, the integral is easily done in that case:

$$m_T = \int_{x_m}^{x_p} a\phi x c_2(x)\, dx = 0 + c_p \phi a \int_x^{x_p} x\, dx$$

$$= \frac{1}{2} a\phi c_p (x_p^2 - \bar{x}^2) \tag{11-19}$$

In the real experiment, the integral

$$m_T = \int_{x_m}^{x_p} a\phi x c_2(x)\, dx \tag{11-20}$$

cannot be performed analytically because $c_2(x)$ is not known explicitly. However, it can be simplified by partial integration:

$$m_T = a\phi c_2(x) x^2/2 \Big]_{x_m}^{x_p} - \frac{1}{2} a\phi \int_{x_m}^{x_p} (\partial c_2/\partial x) x^2\, dx \tag{11-21}$$

After any finite time in the ultracentrifuge at high speeds, $c_2(x_m) = 0$. The first term in Equation 11-21 then is $\frac{1}{2}a\phi c_p x_p^2$. Equating Equations 11-19 and 11-21 and solving for $\bar{x}$, we obtain

$$\bar{x}^2 = (1/c_p) \int_{x_m}^{x_p} (\partial c_2/\partial x) x^2\, dx \tag{11-22}$$

If c_p cannot be measured directly, it can always be obtained as

$$c_p = \int_{x_m}^{x_p} (\partial c_2/\partial x)\, dx \tag{11-22a}$$

Thus, $\bar{x}^2$ is simply the second moment of the concentration gradient distribution. This is not the same as the peak position. In actual experimental sedimentation measurements, $\bar{x}$ generally falls at a slightly larger value of x than the peak in $\partial c/\partial x$. Because Schlieren optics give $\partial c/\partial x$ directly, $\bar{x}$ can be evaluated easily, and a plot of $\ln \bar{x}$ versus time yields the correct sedimentation constant.

Equations 11-16 and 11-18 give two independent measures of the sedimentation constant—one actually determined at the boundary, and the other determined at the plateau. These values should agree, and therefore we can write

$$s = (d\bar{x}/dt)/\omega^2\bar{x} = -(1/2\omega^2 c_p)(dc_p/dt) \tag{11-23}$$

As the boundary moves from x_m to $\bar{x}$, the concentration at the plateau will go from c_0 to c_p, and therefore

$$\int_{x_m}^{x} d(\ln \bar{x}) = -\frac{1}{2} \int_{c_0}^{c_p} d(\ln c_p) \tag{11-24}$$

After integration and rearrangement, we obtain a simple description of radial dilution:

$$c_p/c_0 = (x_m/\bar{x})^2 \tag{11-25}$$

In principle, the detailed shape of the boundary contains information about the diffusion constant of the sedimenting particles (Dishon et al., 1967), and it also can reflect any polydispersity in the sample (Schachman, 1959). In practice, it often is difficult to obtain useful information, because any effects of concentration on s or D are felt very strongly in the boundary region. Before these effects are discussed, it is useful to establish the relationship between s and the properties of individual sedimenting macromolecules. We can do this by simple mechanical considerations.

11-2 ANALYSIS OF SEDIMENTATION MEASUREMENTS

The Svedberg equation

We first consider a mechanical derivation of the relationship between s and molecular properties. There are three forces on a hydrated macromolecule in the plateau region during ultracentrifugation (Fig. 11-9). If M is the anhydrous molecular weight and δ_1

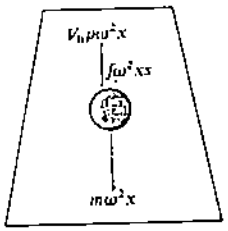

Figure 11-9

Forces on a macromolecule in the ultracentrifuge. The molecule is traveling at the constant velocity $s\omega^2x$. The acceleration force $m\omega^2x$ is balanced by the sum of opposing buoyant and frictional forces. Note that the frictional force $f\omega^2xs$ is actually about one-third the magnitude of the buoyant force $V_h\rho\omega^2x$ for a typical protein.

is the hydration (in g/g), then the total acceleration force F_a on a single particle is $(M/N_0)(1 + \delta_1)\omega^2x$. This force is opposed by two forces. The force due to frictional drag is just $F_f = -fs\omega^2x$. In addition, there is a buoyant force that is proportional to the mass m_s of solution displaced by the macromolecule: $F_b = -m_s\omega^2x$. The displaced solution has a volume equal to the hydrated volume V_h of the macromolecule, which can be calculated from Equation 10-11. If the solution density is ρ, then

$$F_b = -V_h\rho\omega^2x = (M/N_0)(\bar{V}_2 + \delta_1\bar{V}_1)\rho\omega^2x \tag{11-26}$$

The sum of the forces is zero in the hydrodynamic steady state, so

$$(M/N_0)(1 + \delta_1 - \bar{V}_2\rho - \delta_1\bar{V}_1\rho) = sf \tag{11-27}$$

In dilute solution, $\rho^{-1} \cong V_1$, and so the second and fourth terms of the left-hand side of Equation 11-27 cancel, yielding

$$\boxed{s = M(1 - \bar{V}_2\rho)/N_0 f} \tag{11-28}$$

This derivation, although it gives a good mechanical insight, is somewhat fraudulent because of the approximation used to obtain Equation 11-28 from Equation 11-27, and because solution density was used to describe the buoyant force without any real justification. However, the resulting buoyancy term $1 - \bar{V}_2\rho$ is correct, and it does have some interesting consequences. Suppose that $\bar{V}_2 > \rho^{-1}$. This is the case, for example, when lipid-containing samples are placed in aqueous solution. Because the term $1 - \bar{V}_2\rho$ will be negative, in the ultracentrifuge the lipid will float toward the top of the cell rather than sediment toward the bottom.

A more rigorous derivation of Equation 11-28 begins with a thermodynamic description of the flux in a two-component system (Eqn. 11-2). The effect of friction is the only factor connecting flow with the forces due to sedimentation and diffusion. The phenomenological coefficient must be the same as that we evaluated for diffusion alone in Equation 10-61. Thus, $L_{22} = M_2c_2/N_0f$. Therefore, we can write the flux as

$$J_2 = (M_2c_2/N_0f)[\omega^2x - (\bar{c}\hat{\mu}_2/\hat{c}x)] \tag{11-29}$$

In an ultracentrifuge experiment at constant temperature, the thermodynamic variables capable of affecting $\hat{\mu}_2$ are pressure (P) and concentration (c_2). If we consider their effects separately, we have

$$\hat{c}\hat{\mu}_2/\hat{c}x = (\hat{c}\hat{\mu}_2/\hat{c}P)_T(\hat{c}P/\hat{c}x) + (\hat{c}\hat{\mu}_2/\hat{c}c_2)_T(\hat{c}c_2/\hat{c}x) \tag{11-30}$$

The pressure gradient at position x in a solution is simply $\omega^2x\rho$, where ρ is the *solution* density at x, and ω^2x is the accelerating force. The term $\partial\hat{\mu}_2/\partial P$ is defined as the partial specific volume, and this is simply $\bar{V}_2$. The second term in Equation 11-30 was evaluated when diffusion was discussed; for an ideal solution, it is $(RT/M_2c_2)(\hat{c}c_2/\hat{c}x)$. (See Eqns. 10-41 through 10-45). So Equation 11-29 becomes

$$\begin{aligned} J_2 &= (M_2c_2/N_0f)[\omega^2x - \bar{V}_2\rho\omega^2x - (RT/M_2c_2)(\hat{c}c_2/\hat{c}x)] \\ &= [M_2(1 - \bar{V}_2\rho)/N_0f]c_2\omega^2x - (kT/f)(\hat{c}c_2/\partial x) \end{aligned} \tag{11-31}$$

When this expression is combined with the mechanical description of flux (Eqn. 11-4),

it is apparent that

$$\boxed{s = M(1 - \bar{V}_2\rho)/N_0f \quad \text{and} \quad D = kT/f} \tag{11-32}$$

where we have eliminated the subscript 2 on the solute molecular weight.

Note from Equation 11-28 or 11-32 that the sedimentation constant is a function of both the anhydrous molecular weight and the frictional coefficient. In a two-component system, it is the true anhydrous molecular weight that matters, because any acceleration force due to the extra mass of bound water should be canceled by the buoyant force on that bound water. In a multicomponent system, the situation is more complex. There J_2 will depend not only on the forces on component 2, but also on the forces on the third component: $J_2 = L_{22}X_2 + L_{23}X_3$. In addition, $\hat{\mu}_2$ will be a function of the concentration of the third component (c_3). Thus, Equation 11-30 will have an extra term $(\hat{c}\hat{\mu}_2/\hat{c}c_3)(\hat{c}c_3/\hat{c}x)$. Three-component effects can be significant if sedimentation is carried out to concentrated salt solutions. These effects are considered later in this chapter, when density gradient centrifugation is discussed. (Also see Box 11-3.)

In deriving Equation 11-29, we made the tacit assumption that the frictional coefficients affecting diffusion and sedimentation are the same. This identity is not completely rigorous, especially if we want to compare frictional coefficients measured under different conditions: f_D in passive diffusion, and f in the high forces of an ultracentrifuge. For example, a flexible molecule forced to sediment at hundreds of thousands of gravities can distort in shape, thus changing the fractional coefficient. These complications are rare, however. It usually is safe (and always is convenient) to combine the expressions of Equation 11-32 and thus eliminate the frictional coefficient. The result is the Svedberg equation:

$$\boxed{M = sRT/D(1 - \bar{V}_2\rho)} \tag{11-33}$$

Note that the units of R in this equation are cgs: $R = N_0k = 8.31 \times 10^7$ erg mole^{-1} deg^{-1}.

Determining molecular weights from sedimentation data

The Svedberg equation permits an unambiguous determination of the molecular weight, independent of any details of shape—providing that separate sedimentation, diffusion, and partial-specific-volume measurements can be performed on equivalent

samples under conditions as similar as possible. In practice, the conditions used for the three measurements rarely are identical. It is customary to correct sedimentation data to the values that would be observed if the measurements had been performed at 20°C in pure water.

The corrections for diffusion are given in Equation 10-67. The corresponding corrections for sedimentation are calculated by noting (from Eqn. 11-32) that s will depend on solvent and temperature (because $\bar{V}_2$ and ρ are functions of these variables) and on the viscosity η (because f depends on viscosity; see Eqn. 10-68). Therefore, the ratio of the sedimentation constant measured in water at 20°C to that measured under different conditions will be

$$\frac{s_{20,w}}{s} = \frac{1 - 0.9982(\bar{V}_2)_{20,w}}{1 - \bar{V}_2\rho}\left(\frac{\eta_{T,w}}{\eta_{20,w}}\right)\left(\frac{\eta_{T,soln}}{\eta_{T,w}}\right) \tag{11-34}$$

where the subscripts soln and T represent the actual sample solution and temperature used; $\eta_{T,w}$ is the viscosity of pure water at temperature T: $\eta_{20,w}$ is 0.01002 poise; 0.9982 g cm^{-3} is the density of water at 20°C; and $(\bar{V}_2)_{20,w}$ is the partial specific volume measured in water at 20°C.

The sedimentation and diffusion coefficients, although assumed constant in most of the equations derived in this chapter, actually are concentration-dependent in practice. Therefore, it is common (and often is necessary) to measure s and D as functions of concentration and then to extrapolate to infinite dilution to obtain s^0 and D^0; these quantities then are corrected to the values expected at 20°C in pure water at infinite dilution: $s^0_{20,w}$ and $D^0_{20,w}$.

Table 11-1 shows some typical measured values of $s_{20,w}$. What can be done with these values depends on what else is known about the system. If the molecular weight is known, a determination of $s_{20,w}$ yields the frictional coefficient f, which can be compared to f_{min}, the coefficient expected for an anhydrous sphere. The ratio

Table 11-1
Results of sedimentation measurements

Sample	Molecular weight	$s_{20,w}$ (S)	$\bar{V}_2$ (cm^3 g^{-1})	f/f_{min} (sedimentation)	f/f_{min} (diffusion)
Ribonuclease A (bovine)	12,400	1.85	0.728	1.29	1.14
Lysozyme (chicken)	14,100	1.91	0.688	1.22	1.32
Serum albumin (bovine)	66,500	4.31	0.734	1.33	1.31
Hemoglobin	68,000	4.31	0.749	1.28	1.14
Tropomyosin	93,000	2.6	0.71	2.65	3.22
Fibrinogen (human)	330,000	7.6	0.706	2.34	2.35
Myosin (rod)	570,000	6.43	0.728	3.63	3.05
Bushy stunt virus	10,700,000	132.	0.74	1.27	1.27
Tobacco mosaic virus	40,000,000	192.	0.73	2.65	2.19

SOURCE: Data from several sources, including Kuntz and Kauzmann (1974), Tanford (1961), and Van Holde (1971).

f/f_{min} can be analyzed in turn to obtain limits on shape and hydration, exactly as described earlier for diffusion coefficients. A comparison of frictional coefficients derived from diffusion and from sedimentation is shown in Table 11-1. The agreement is fairly good in most cases. If both $s_{20,w}$ and $D_{20,w}$ are known, the molecular weight can be computed from Equation 11-33. Then either expression of Equation 11-32 would yield the frictional coefficient. Unfortunately, because sedimentation and diffusion give the same measure of combined shape and hydration, a knowledge of both quantities does not resolve ambiguities as to how much of the excess friction (over f_{min}) is due to hydration. Table 11-2 compares molecular weights obtained using the Svedberg equation with values determined by other techniques. The various methods generally are quite consistent. They should not agree exactly for a number of reasons, including the fact that counterions are weighted to different extents by some of the methods.

Table 11-2
Molecular weights determined by various methods

Sample	Chemical structure	Sedimentation and diffusion	Archibald	Sedimentation equilibrium	Scheraga-Mandelkern	Other
Sucrose	342.3	—	—	341.5	—	—
Raffinose	504.5	—	495	—	—	—
Ribonuclease A (bovine)	13,683	12,400	13,750	13,700	15,200	—
Lysozyme (chicken)	14,211	14,100	—	14,500	12,400	14,100[1]
Serum albumin (bovine)	66,296	66,000	70,000	68,000	59,000	70,000[2]

[1] From small-angle x-ray measurements.
[2] From light-scattering measurements.

Equation 11-33 cannot be used as often as one would like, because diffusion measurements are not that common. It is possible to combine sedimentation data with other hydrodynamic measurements, as will be demonstrated later. All too frequently, a sedimentation coefficient is the only hydrodynamic information available on a system of unknown molecular weight. This is because sedimentation experiments either are faster or require less sample than most other methods. Less than 0.1 mg of a protein (and an order of magnitude less of nucleic acid) can suffice for the determination of $s_{20,w}$ using sensitive photoelectric scanning detection. The actual measurement takes less than a few hours, during which time the boundary moves on the order of a centimeter. This distance can be measured very accurately.

Easy as it is to obtain, a value of $s_{20,w}$ alone requires that some guess be made about either shape or molecular weight in order to estimate the other quantity. If the macromolecule is a sphere, substitution of Equations 10-68 and 10-69 into Equation 11-28 (with the Perrin shape factor $F = 1$) yields

$$s = (M^{2/3}/N_0^{2/3})(1 - \bar{V}_2\rho)\{6\pi\eta[(3/4\pi)(\bar{V}_1 + \delta_1\bar{V}_1)]^{1/3}\}^{-1} \tag{11-35}$$

The sedimentation constant for spherical molecules with similar hydration and partial specific volumes is proportional to $M^{2/3}$. This is a very useful result. If, for example, different associated forms of protein subunits are studied, their molecular weights can easily be related by sedimentation measurements, providing that none of the forms is too aspherical. Equation 11-35 is used in a wide variety of cases to estimate molecular weights by guessing values of the hydration. These estimates are fairly valuable for most cases but, in any given case, the prudent investigator will be somewhat cautious.

Shape information from sedimentation data

The shape-dependent predictions of hydrodynamic theory can be tested by using a homologous series of molecules identical in all respects except length. A convenient system, used for this purpose by B. D. Harrison and A. Klug, is tobacco rattle virus (TRV). The infective virus is a cylinder 250 Å in diameter and 1,850 to 1,970 Å long. However, infection also produces shorter particles that can be isolated and studied.

To treat a homologous series, it is convenient to write the frictional coefficient in the form $f = 6\pi\eta(3V_e/4\pi)^{1/3}F$, where V_e is the volume of the equivalent hydrated sphere, and F is a shape factor. The actual volume for a cylindrical rod is $\pi r^2 l$, where l is the length and r is the radius. Using these expressions for f and V_e, we can rewrite Equation 11-28 as follows:

$$M/l = \{[6\pi\eta N_0(3r^2/4)^{1/3}]/(1 - \bar{V}_2\rho)\}(sF/l^{2/3}) \tag{11-36}$$

The molecular weight per unit length (M/l) is constant for a series of homologous rods. Similarly, the first term on the right-hand side is a constant. Therefore, the prediction is that $sF/l^{2/3}$ should be a constant. Figure 11-10a shows a test of this prediction. The prediction is fairly accurate, using Perrin F values for prolate ellipsoids with axial ratios of $l/2r$.

An even better fit is obtained if rods are modeled slightly more realistically. The volume of a prolate 2 ellipsoid is $4\pi ab^2/3$, where a is the major semiaxis, and b is the minor semiaxis. The volume of a cylinder is $\pi r^2 l$. We must set these two volumes equal, to ensure that there are equal numbers of particles in the solution for a given fixed weight concentration.

$$\pi r^2 l = 4\pi ab^2/3 \tag{11-37}$$

Now, selecting an ellipsoid with the same length as the rod: $l = 2a$. Therefore Equation 11-37 can be put in the following form:

$$l/a = 2 = 4b^2/3r^2 = (1/3)(b^2/r^2)(l^2/a^2) \tag{11-38}$$

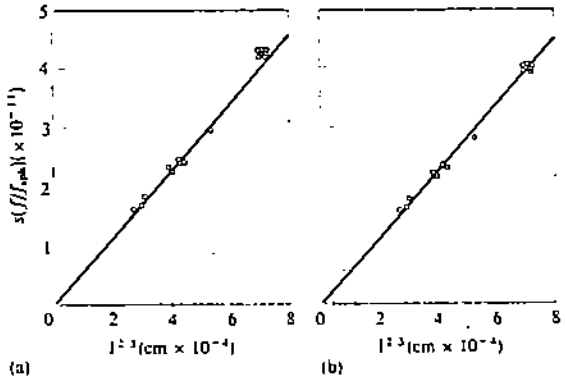

Figure 11-10

Sedimentation coefficient of TRV (tobacco rattle virus) particles as a function of length. Lengths (l) were measured in the electron microscope, and these dimensions were used to calculate f/f_{sph} for prolate ellipsoids. The actual plots used here show (measured length)$^{2/3}$ versus measured s times calculated f/f_{sph}. (a) The axial ratio for ellipsoid is calculated as l/d, where d is the diameter of the rod. (b) The axial ratio is calculated as $\sqrt{2/3}\,l/d$. [After B. D. Harrison and A. Klug, *Virology* 30:738 (1966).]

The second and fourth expressions can be rearranged to give

$$a/b = l/6^{1/2}r = (2/3)^{1/2}(l/d) \tag{11-39}$$

where $d = 2r$ is the diameter of the rod. Therefore, an ellipsoid is chosen with an axial ratio slightly smaller than that of the rod. When this is done, the fit of Equation 11-36 to experimental data is nearly perfect (Fig. 11-10b).

The accuracy of sedimentation measurements permits their use in fairly exacting structural discriminations. Hemoglobin has a measured sedimentation constant of about 4.45 S. Each of its four subunits (two α and two β) has an individual sedimentation constant of about 1.77 ± 0.055 S. One can calculate the sedimentation constant of a tetramer from monomer properties using the Kirkwood–Riseman theory (Section 10-2). If both the tetramer (t) and monomer (m) have the same $\bar{V}_2$, one can write (from Equation 11-28)

$$s_t/s_m = (M_t/M_m)/(f_t/f_m) = 4f_m/f_t \tag{11-40}$$

where f_m/f_t is given by Equation 10-34 and must be computed for a specific geometric model of the tetramer. Using the measured monomer sedimentation constant and

the values of f/f_m shown in Figure 10-12, we can predict that $s = 3.91 \pm 0.11$ S for a linear tetramer; $s = 4.18 \pm 0.12$ S for a square planar tetramer; and $s = 4.43 \pm 0.13$ S for a tetrahedral tetramer. Thus the data yield sufficient precision to permit the correct deduction that hemoglobin has a tetrahedral arrangement of subunits. Figure 11-11 shows the results of a more complicated example of the use of the Kirkwood–Riseman theory.

To use sedimentation as a monitor of conformational change, it is convenient to make the most precise possible measurements of the difference in sedimentation of two samples of the same substance under slightly different conditions. An effective technique for the purpose is difference sedimentation. The cell used has two identical sector-shaped sample chambers placed side by side (the double-sector counterpiece in Fig. 11-3b). The samples to be compared are placed in the separated sectors and are spun together. Optical systems are used to detect just the differences between the two sectors, in much the same way as difference spectroscopy is carried out. It turns out to be particularly convenient to use Rayleigh optics, which give the differences in solute concentration in the two sectors as a function of position. This technique permits measurement of sedimentation-constant differences as small as 0.01 S with better than 1% precision. However, it places very stringent requirements on the optical system, and these preclude routine use.

Effects of concentration on sedimentation velocity

Everything we have said thus far is applicable to a two-component system (water plus macromolecule) in the limit of great dilution. Formidable difficulties can occur

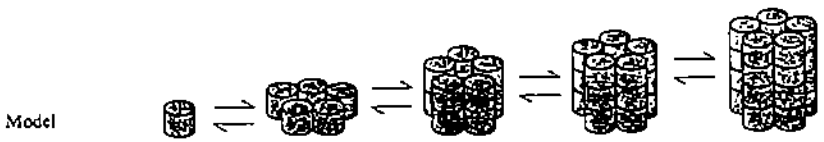

Model					
No. of units	1	5	10	15	20
s (predicted)	20 S	59 S	100 S	131 S	156 S
s (obs) (loligo)	19 S	59 S	97 S	—	—
s (obs) (busycon)	—	60 S	100 S	130 S	155 S

Figure 11-11

Measured and predicted sedimentation constants for two species of molluscan hemocyanins (loligo and busycon). The Kirkwood–Riseman theory was used to calculate the predicted values for the oligomeric models shown. [After V. Bloomfield, W. O. Dalton, and K. E. Van Holde, *Biopolymers* 5:135 (1967).]

when these conditions are not met. Here we provide a brief sketch of some of the more commonly encountered effects.

Even in a two-component system, the sedimentation velocity is a function of solute concentration. The dependence of sedimentation on concentration for a single macromolecular component generally can be fit to equations of the form

$$s = s^0(1 + k'c)^{-1} \tag{11-41}$$

or

$$s = s^0(1 - k''c) \tag{11-42}$$

where s^0 is the value at infinite dilution, and k' and k'' are empirically derived constants. Both equations account for a decrease in observed sedimentation velocity with increasing concentration (Fig. 11-12). With small values of c, the equations are

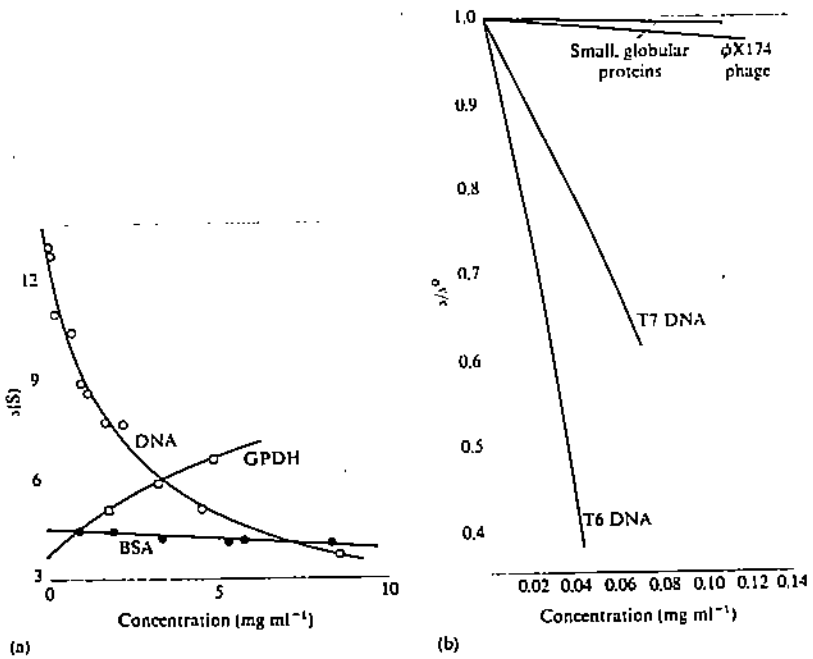

Figure 11-12

Concentration dependence of the sedimentation constant. (a) Actual sedimentation data for three macromolecules: DNA of about 3×10^6 mol wt, bovine serum albumin (BSA), and glycerol phosphate dehydrogenase (GPDH). [After C. Tanford (1961), K. E. Van Holde (1971).] (b) Relative sedimentation data for several other molecules. Note that the concentration dependence becomes more severe as the molecular weight increases. For example, T7 DNA has a molecular weight of 2.5×10^7 d. [After D. Freifelder, *Physical Biochemistry*, p. 285. (San Francisco: W. H. Freeman and Company.) Copyright © 1976.]

equivalent, because $(1 + kc)^{-1} = 1 - kc +$ (terms of higher order in c). However, the two expressions predict very different behavior at high concentrations.

The physical justification of the two equations also is very different. Equation 11-41 is the form expected if the major effect of solute concentration is to alter the frictional properties of the solution. The sedimentation constant is proportional to f^{-1}, and f is proportional to the solution viscosity. As shown in Chapter 12, η can always be written as a power series in the concentration of solute. The first two terms are $\eta = \eta_0(1 + [\eta]c)$, where η_0 is the viscosity of pure solvent, and $[\eta]$ is called the intrinsic viscosity. Combining this expression with Equation 10-68, inserting the result into Equation 11-28, and ignoring the effects of concentration on density, we obtain Equation 11-41 with $k' = [\eta]$. In practice, however, this equation usually does not fit the observed data very well. Except for DNA, experimentally determined values of k' often are larger than those of $[\eta]$.

Equation 11-42 is the form expected if backward flow of solvent is the major force that slows down sedimentation with increasing solute concentration. For example, a spherical particle drags about four times its own volume of solvent with it. Thus, during the sedimentation of a macromolecule, a considerably larger volume of solvent must flow in the cell in the direction opposite to that of sedimentation. This flow will be proportional to the volume of the sedimenting macromolecules multiplied by their velocity. As viewed by an observer outside the cell, the macromolecules will appear to be moving more slowly. They are, in effect, swimming upstream. As we shall show in Chapter 12, the constant $[\eta]$ in a power expansion of the viscosity is proportional to the volume fraction occupied by solute. Therefore, k' and k'' are related, and they become equivalent in the limit of low concentration. At high concentration, neither Equation 11-41 nor Equation 11-42 can account very well for experimental data, and more complicated expressions are needed.

The effect of solute concentration on the shape of the boundary observed in a sedimentation experiment can be dramatic. When a concentrated DNA solution is centrifuged, molecules in the plateau will sediment slowly (as shown in Fig. 11-12) because they feel the full effect of the high concentration. Suppose there were a broad boundary (Fig. 11-13a). The DNA molecules at the trailing edge are at very low concentration. They should be sedimenting very fast. If they do this, they catch up with the molecules at the leading edge of the boundary. The result is that a broad boundary cannot form, even if diffusion is considerable. Instead, the boundary self-sharpens and remains sharp upon further sedimentation (Fig. 11-13b). This can hide the effect of any heterogeneity of molecular weight in the sample.

Effect of self-association on sedimentation velocity

One of the experimental samples in Figure 11-12 has a sedimentation constant that increases with increasing concentration. From an argument exactly opposite to that used for self-sharpening boundaries, one can predict that the boundary should broaden in this case. Indeed, this is the observed result, but what is its origin? Suppose that a protein monomer P can associate to form oligomers such as $2\,P \rightleftharpoons P_2$, or even large aggregates such as $n\,P \rightleftharpoons P_n$. If the rates of interconversion are infinitely slow (on the time scale of the sedimentation experiment), then two boundaries should be seen—one corresponding to P and one to P_2 (or P_n).

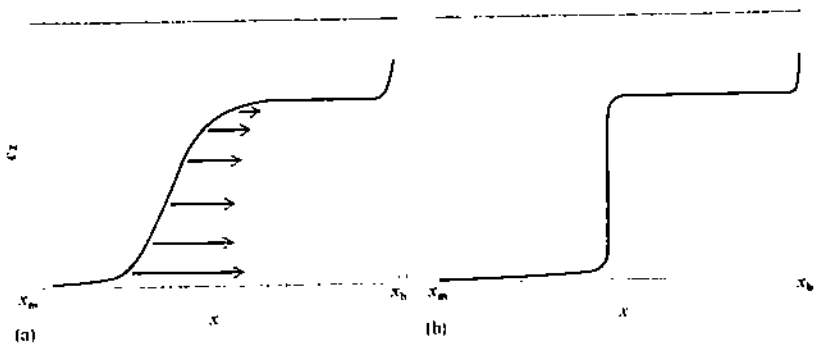

Figure 11-13

Self-sharpening boundary. **(a)** Assume a broad boundary formed in a concentrated solution of DNA. The concentration dependence of s shown in Figure 11-12 would mean that different points of the boundary would move at very different velocities. **(b)** In concentrated DNA, the broad boundary is never actually seen. Instead, a hypersharp boundary forms, stabilized by the effects shown in part a.

At faster rates of interconversion, for a monomer–dimer equilibrium, the two boundaries merge into one asymmetric boundary. Even if concentration effects on intrinsic sedimentation rates are ignored, this boundary will have a complex shape that can be analyzed by the theory developed by G. A. Gilbert (see Cann, 1970; Van Holde, 1975). The total solute concentration is near zero at the trailing edge of the boundary, and the equilibrium will favor the monomer. The dimer can be favored if the concentration is high enough at the leading edge. The resulting boundary will be asymmetric, and the position of maximal $\partial c/\partial x$ will be a function of the extent to which the equilibrium favors monomer or dimer.

For a rapid monomer–n-mer equilibrium (with $n > 2$), two boundaries will be seen in certain concentration ranges, and the relative height of the faster-moving boundary will increase with increasing concentration. In the limits of low or high concentrations, a single asymmetric boundary will result. If there are only two species, it sometimes is possible to determine the molecular weight of the aggregate (and even information about the association constant) by analyzing the relative positions and heights of the boundaries. However, in general, an exact analysis of boundary shape in systems with reacting species is a formidable problem that still taxes current research.

Regardless of what is happening at the boundary, some information is available in a straightforward manner from the plateau region. Whether the system is a mix-

ture of interacting or of noninteracting components, one still can describe the flux in the plateau (or in the final plateau, past any and all observed boundaries) from Equation 11-4 as

$$J_p = \omega^2 x \sum_i c_i s_i \tag{11-43}$$

where c_i is the weight concentration of material with sedimentation constant s_i, and diffusion is neglected because $\sum_i (\partial c_i/\partial x_i) = 0$. By analogy to Equation 11-16, the concentration change with time at the plateau then becomes

$$dc_p/dt = d\left(\sum_i c_i\right)\Big/dt = -2\omega^2 \sum_i c_i s_i \tag{11-44}$$

The value of dc_p/dt is an experimentally observable quantity. If one did not know there was a mixture, one would associate it with an apparent sedimentation constant $\bar{s}$:

$$dc_p/dt = -2\omega^2 \bar{s} c_p = -2\omega^2 \bar{s} \sum_i c_i \tag{11-45}$$

Equating the right-hand sides of Equations 11-44 and 11-45, you can see that the apparent sedimentation constant that will be measured is $\bar{s} = \sum_i s_i c_i / \sum_i c_i$. Because c_i is in weight units, $\bar{s}$ is the weight-average sedimentation constant. For some applications, $\bar{s}$ is useful, but much information about the system is lost in performing the average.

Effects of multiple macromolecular components on sedimentation velocity

If a mixture of more than one macromolecule type is sedimented, more than one boundary generally will be seen. However, the analysis of boundaries in multicomponent systems becomes very complicated. The concentration dependence of sedimentation in a mixture with two or more components is a function of all the components in a given region. Among other things, this means that the backward flow created by a fast component can be felt by a slow component, and in some cases can even overwhelm the sedimentation of the slow component.

To highlight this effect, we consider a somewhat unusual case in which the fast boundary is nearer the rotation axis than is the slow boundary. This effect can be produced at short times in the centrifuge by using a synthetic boundary cell (Fig. 11-14a). This is a double-sector cell made with thin channels connecting the two sectors. At normal gravity, hydrostatic pressure is insufficient to overcome the resistance of these channels to flow. Once in the centrifuge, the hydrostatic forces become

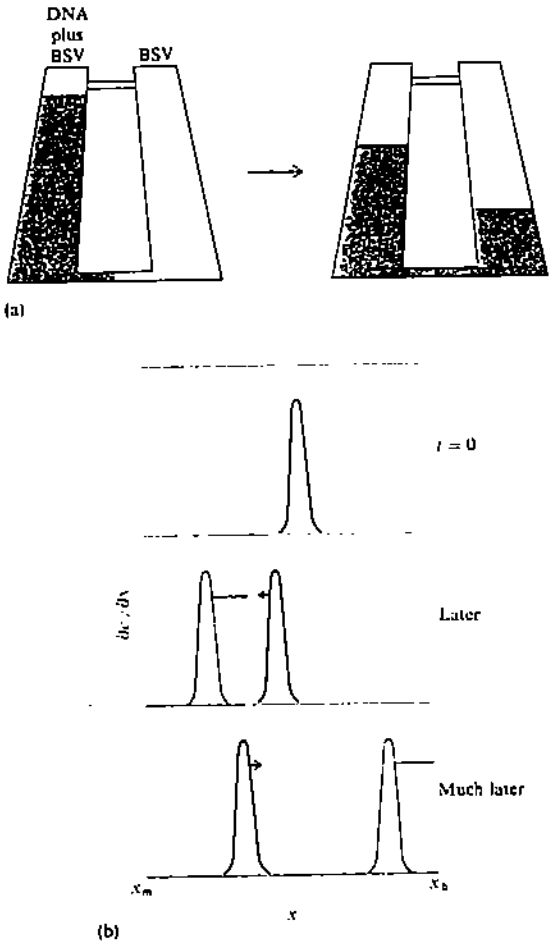

Figure 11-14

Demonstration of solvent backward flow. (a) A synthetic-boundary cell is loaded with separate samples of pure bushy stunt virus (BSV) and a virus–DNA mixture. In the ultracentrifuge, hydrostatic forces equalize the fluid levels in the two sectors, resulting in a DNA boundary in the center of the right-hand sector. (b) Sedimentation profiles seen in the right-hand sector as a function of time after fluid flow between the sectors. The initial DNA boundary moves up until the BSV boundary passes it. Then it reverses direction and sediments toward the bottom.

enormous, and any differences in the heights of the fluid in the two sectors are eliminated by flow through the channels.

To make a synthetic boundary of slowly sedimenting DNA in the middle of a uniform solution of bushy stunt virus (BSV), one places a small volume of BSV solution in one sector and a large volume of BSV at the same concentration containing added DNA in the second sector. Figure 11-14 shows that, after a very short time, fluid flow produces in one sector a DNA boundary in the midst of a uniform BSV concentration. This sector is used for further examination. The BSV rapidly forms a boundary near the meniscus, and this boundary travels down the cell at about 120 S. When measured separately, the DNA used would move down with a sedimentation constant of about 10 S. However, in this experiment, it actually moves up with a constant of about -10 S in the presence of the sedimenting BSV. Thus, the backward flow experienced by the DNA is about 20 S. The schematic illustration of Figure 11-14b is an oversimplification, however, because it ignores another effect.

The size of a boundary is $\int(\partial c/\partial x)dx$; in a one-component system, this size is simply c_p and is a measure of concentration at the plateau. It has long been known that, when mixtures of two components are sedimented, the boundary sizes do not correctly correspond to the fractional composition. This is called the Johnston–Ogston effect. To simplify the explanation of this effect, our discussion here ignores radial dilution. The fast component always sediments in the presence of the slow with a rate s_F (Fig. 11-15a). However, the slow component must sediment at different rates: s_S above the fast-component boundary, where it feels only its own concentration, and $s_{S,F}$ below that boundary, where both fast and slow components are present. Equation 11-41 or 11-42 ensures that $s_{S,F} < s_S$, but this has serious consequences. Imagine

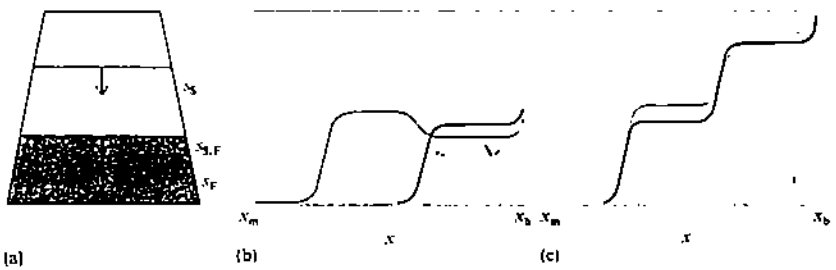

Figure 11-15

The Johnston–Ogston effect in a two-component system. (a) The sedimentation velocity of the slow component decreases at the fast-component boundary, because of the higher total solute concentration below that boundary. (b) Sedimentation profiles expected if the fast and slow components could be measured separately. (c) Sedimentation profile of the sum of the two components. The colored line shows the actual profile; the black line shows the profile that would be expected if the Johnston–Ogston effect could be neglected.

sitting on the *moving* fast boundary and watching the fluxes of slow component. Looking toward the top of the cell, we would see slow component moving away with a flux $J = \omega^2 x(s_F - s_S)c_S$. Looking toward the bottom, we would see slow component approaching with $J' = \omega^2 x(s_F - s_{S,F})c_{S,F}$. Therefore, J' is larger than J, implying that slow substance should accumulate continuously at the fast boundary. Such accumulation is impossible, because it would lead to a high local density. The fast component would slow down because of the $1 - \bar{V}_1\rho$ term in Equation 11-28, and a gravitation instability would result as well. The boundary would be denser than the solution below it, and it would fall to the bottom by convective mixing.

What happens instead, when the problem is properly solved, is that the concentration of the slow component readjusts to prevent this catastrophe. For there to be no flux change in the slow component at the fast boundary, $J = J'$, which means that

$$c_{S,F}(s_F - s_{S,F}) = c_S(s_F - s_S) \tag{11-46}$$

Because $s_{S,F} < s_S$, the concentration c_S of the slow component above the fast boundary is greater than the concentration $c_{S,F}$ below the boundary (Fig. 11-15b). The result is a slow boundary larger than naively expected and a fast boundary smaller than expected, because most optical monitoring techniques detect the sum of the concentrations of both components.

Zonal sedimentation of multicomponent systems

The Johnson–Ogston effect and other multicomponent effects are particularly troublesome in velocity sedimentation because all components, except the slowest one, are always present as mixtures. This also means that sedimentation, as described thus far, is rather ineffective at separating or purifying components, unless their sedimentation rates are very different.

The technique of zonal sedimentation circumvents both of these problems. A thin band of macromolecule sample is layered on top of a much larger volume of solvent. This can be done in the analytical ultracentrifuge by using a band-forming centerpiece (Fig. 11-16a), which is similar in principle to the synthetic boundary cell described earlier. A mixture of several components with different sedimentation constants will rapidly separate into bands of pure components. Each will travel at its characteristic sedimentation velocity. Diffusion will broaden each band into a Gaussian shape (Eqn. B of Box 10-3). In practice, the shapes are more complicated. Because the acceleration force increases as $\omega^2 x$, the leading edge of a band will travel faster than the trailing edge. The concentration dependence of sedimentation further distorts the band shape. The concentration is low at the leading and trailing edges, and molecules move rapidly. The concentration is high in the center of a band, and velocities are slower. The result is a band with a broad leading edge and a sharp trailing edge (Fig. 11-16b).

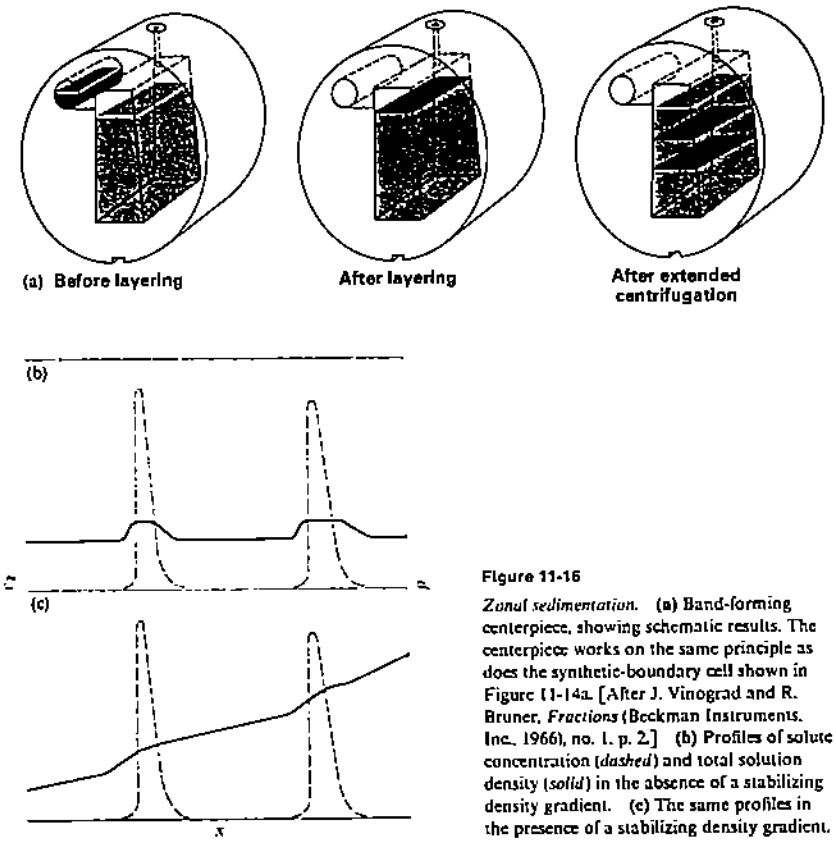

Figure 11-16

Zonal sedimentation. **(a)** Band-forming centerpiece, showing schematic results. The centerpiece works on the same principle as does the synthetic-boundary cell shown in Figure 11-14a. [After J. Vinograd and R. Bruner, *Fractions* (Beckman Instruments, Inc., 1966), no. 1, p. 2.] **(b)** Profiles of solute concentration (*dashed*) and total solution density (*solid*) in the absence of a stabilizing density gradient. **(c)** The same profiles in the presence of a stabilizing density gradient.

Note one major advantage of zonal sedimentation. All of the biological sample is concentrated into a small volume. This substantially enhances the ability to detect the sample. Therefore, much smaller samples can be used with zonal sedimentation than with other techniques; for example, less than 1 μg of DNA will suffice to measure a zone.

Zonal sedimentation would be impossible in a homogeneous solution because of gravitational instabilities. The density of the sample would be higher in a band than in the solution below it, and the bulk solution region containing the band would simply collapse. For example, a DNA solution with concentration 0.01 mg ml^{-1} would have a density roughly 2×10^{-5} g cm^{-3} larger than that of the solvent. However, this density difference is magnified by the 4×10^5 *g* forces typical in the ultracentrifuge. The result is roughly equivalent to trying to float mercury on top of water. It doesn't work.

A density gradient must be created in the solvent to eliminate this problem. This can be done with the moderately dilute salt solutions used in the analytical ultracentrifuge by having the original sample in a more dilute salt. When the sample transfers in a zone on top of the bulk solvent, rapid small molecule diffusion creates a shallow density gradient (Fig. 11-16b). This gradient can differ as little as 1% from top to bottom of the cell. Thus, it does not perturb sedimentation velocities too seriously. The gradient will be stabilized (and even enhanced) in the ultracentrifuge, because salt molecules are denser than water. The high forces in the ultracentrifuge can be felt even by small ions. However, these dilute salt gradients are not very stable outside of the centrifuge. If one wanted to recover a pure, separated band, it would be necessary to pump it out while the rotor was still spinning. This is possible, but there is a simpler solution in most cases.

Preparative zonal sedimentation is mainly a purification technique. A preformed gradient of a somewhat viscous solute is used. A linear gradient of 5% to 20% sucrose is typical. Glycerol is another common solute. A linear gradient is easy to prepare using the mixing device shown in Figure 11-17 (see Box 11-2). Such a gradient is

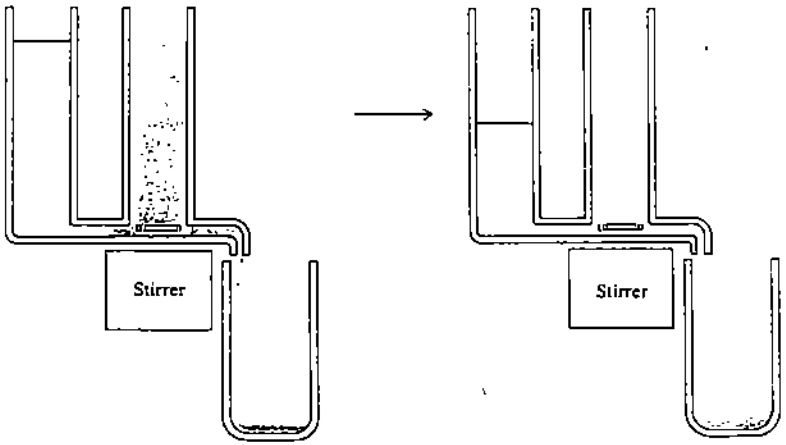

Figure 11-17

Apparatus for generation of a linear density gradient. The right-hand vessel is assumed to be stirred to homogeneity at all times.

more stable outside the centrifuge than a dilute salt gradient, and it will remain fairly constant in the ultracentrifuge because the viscosity of the concentrated sucrose impedes redistribution. Therefore, a sample can be layered on top of the preformed gradient in a centrifuge tube so long as its density is less than that at the top of the gradient. The solute molecules of the sample will sediment through the gradient because $(1 - \bar{V}_2\rho)$ is greater than zero throughout. After spinning for a time sufficient to move the solute molecules part of the way down the centrifuge tube, the centrifuge is stopped. The gradient is collected and gently removed from the tube, either by puncturing the bottom and allowing it to drop out, or by pumping in more dense sucrose at the bottom and displacing the gradient out the top. Individual fractions are collected and analyzed in any way one wishes.

It is very difficult to determine an absolute sedimentation constant by the analysis of a sucrose gradient. Only a single time point is available, so there are uncertainties in the meaning of the band position, because acceleration and deceleration times of the rotor may not be known with any accuracy. More serious is the direct effect of the sucrose itself. The density and viscosity of the solution are not constant, and therefore s is not constant. Thus Equation 11-18 cannot be used to compute s. In practice, standards usually are run along with an unknown sample. Convenient standards are enzymes or isotopically labeled substances that can be added in trace amounts and subsequently assayed after the gradient has been fractionated. It is a common practice to determine the sedimentation constant of an unknown by bracketing it between two standards of known $s_{20,w}$ and assuming that s is a linear function of the distance between the two standards. This assumption is not correct for most gradients, and the procedure should be used only when the standards are virtually coincident with the unknown.

If accurate sedimentation constants must be obtained through preparative gradient centrifugation, the best procedure is to construct an isokinetic gradient. This gradient is designed so that $[1 - \bar{V}_2\rho(x)]$, $[\eta(x)]$ cancels the x-dependence of the accelerating force. It can be approximated by a properly chosen exponential gradient of a solute that affects both ρ and η linearly with concentration. Then the sedimentation constant will be a linear function of the distance traveled. One still must worry about attempting to match the $\bar{V}_2$ values of samples and standards. One also must realize that there could be significant three-component thermodynamic effects in concentrated sucrose. However, when properly used, sucrose-gradient sedimentation is a powerful analytical tool.

ox 11-2 THE GRADIENT PRODUCED BY A MIXING CHAMBER

he mixing-chamber apparatus is illustrated in Figure 11-17. We wish to show that a linear oncentration gradient will be delivered to the tube. Because the heights of the two mixing essels must remain equal, the volume of solution in the right-hand container is $V_R = V_0 - V_d$, where V_0 is the initial volume, and V_d is the volume that has dripped into the tube. The ass of solute in the right-hand container is $M_R = c_R V_R$, where c_R is the concentration in the ight-hand container. The rate of mass change with each drop must be $dM_R/dV_d = -c_R + \frac{1}{2}c_L$, ecause the right-hand vessel loses one drop of its contents at c_R, but gains one-half drop rom the left-hand vessel at concentration c_L. However, one also can evaluate this derivative rom the chain rule:

$$dM_R/dV_d = V_R(dc_R/dV_d) + c_R(dV_R/dV_d)$$
$$= (V_0 - \tfrac{1}{2}V_d)(dc_R/dV_d) - \tfrac{1}{2}c_R$$

Equating the two expressions for dM_R/dV_d, we obtain a simple differential equation:

$$-2dc_R/(c_R - c_L) = dV_d/(V_0 - \tfrac{1}{2}V_d)$$

Integration from $c_R(0)$ to $c_R(V_d)$, as V_d goes from 0 to V_d, yields

$$[c_R(V_d) - c_L]/[c_R(0) - c_L] = 1 - V_d/2V_0$$

The concentration decreases linearly in the right-hand vessel as solution drips into the tube, and therefore the concentration in the tube must decrease linearly with height.

11-3 EQUILIBRIUM ULTRACENTRIFUGATION

Suppose a macromolecule is subjected to ultracentrifugation at speeds insufficient to transport it to a packed band at the bottom of the cell. Some transport must occur, but eventually an equilibrium will be established (Fig. 11-18). Solute is removed from

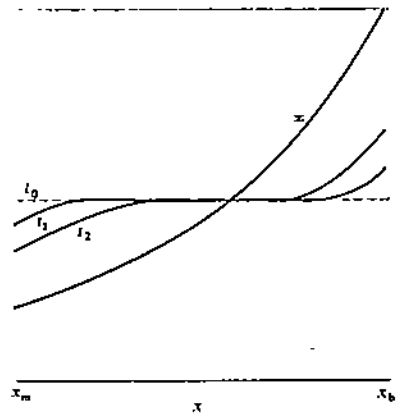

Figure 11-18
Sedimentation to an equilibrium solute distribution. [After C. Tanford, *Physical Chemistry of Macromolecules* (New York: Wiley, 1961), p. 385.]

the meniscus region as time progresses, and it tends to accumulate near the bottom of the cell. Diffusion forces are too strong to let a boundary be formed, and so a smooth concentration gradient eventually develops throughout the cell. The time required for this gradient to reach equilibrium can be shown to depend on $(x_m - x_b)^2$. For the standard sector-shaped centerpieces used in velocity sedimentation, this time is impractically long; however, the time can be brought within practical limits by the use of much shorter column heights.

Determining molecular weight with equilibrium ultracentrifugation

At equilibrium, the solute flux J_2 must be zero everywhere in the sample. Using either Equation 11-31 (corrected for nonideality) or Equation 11-4 and the appropriate molecular expressions for s and D, we can write

$$[c_2\omega^2 xM(1 - \bar{V}_2\rho)]/N_0 f = (kT/f)[1 + \partial(\ln \gamma_2)/\partial(\ln c_2)](\partial c_2/\partial x) \quad (11\text{-}47)$$

Rearranging to place all measurable quantities on one side, and canceling f, we obtain

$$M[1 + \partial(\ln \gamma_2)/\partial(\ln c_2)]^{-1} = [RT/(1 - \bar{V}_2\rho)\omega^2](1/c_2 x)(\partial c_2/\partial x) = [2RT/(1 - \bar{V}_2\rho)\omega^2][\partial(\ln c_2)/\partial x^2] \quad (11\text{-}48)$$

Note that only thermodynamic variables such as T and $\bar{V}_2$ remain. This is as it should be; the frictional coefficient can have no role at equilibrium. In ideal solutions, or at low concentrations, the activity-coefficient term vanishes, and Equation 11-48 can be integrated, using as a boundary condition the concentration c_2 at some reference point x_0:

$$c_2(x) = c_2(x_0)\exp\{[M(1 - \bar{V}_2\rho)\omega^2/2RT(x^2 - x_0^2)\} \quad (11\text{-}49)$$

Equations 11-48 and 11-49 imply that the slope of a plot of $\ln c_2$ versus x^2 is all that is needed to measure the molecular weight.

Equation 11-49 can be used to estimate the rotation speed needed for an equilibrium measurement. With a typical optical system, accurate measurements can be made when the solute concentration falls by a factor of two across a 1 mm sample height. If $M = 50{,}000$ d, and $x_0 = 6$ cm, and $\bar{V}_2 = 0.75$ cm^3 g^{-1}, then ω is 10,400 rpm. This centrifuge speed is 5-fold slower (and the resulting forces are 25-fold weaker) than what is used for typical velocity sedimentation experiments.

Conservation of mass can be used to provide an alternative form of Equation 11-49 that is useful for determining molecular weight. The total solute in the cell at equilibrium must be equal to the total that was initially present. The initial weight

of solute is

$$\int_{x_m}^{x_b} \phi a c_0 x\,dx = \frac{1}{2}\phi a c_0(x_b^2 - x_m^2) \quad (11\text{-}50)$$

where c_0 is the uniform initial concentration. The total mass present at equilibrium can be obtained by rearranging the first and second expressions of Equation 11-48 and integrating. For ideal solutions, we obtain

$$\phi a\int_{x_m}^{x_b} c_2(x)x\,dx = [RT/M(1 - \bar{V}_2\rho)\omega^2]\phi a\int_{x_m}^{x_b} dc_2 = [RT/M(1 - \bar{V}_2\rho)\omega^2]\phi a(c_b - c_m) \quad (11\text{-}51)$$

where c_b and c_m are the solute concentrations at the bottom and at the meniscus, respectively. Setting Equations 11-50 and 11-51 equal, we obtain an expression for the molecular weight that depends only on concentration ratios:

$$(c_b - c_m)/c_0 = M(1 - \bar{V}_2\rho)\omega^2(x_b^2 - x_m^2)/2RT \quad (11\text{-}52)$$

In practice, the use of Equation 11-49 or 11-52 is complicated by the difficulty of making actual concentration measurements in the ultracentrifuge. Some optical methods give only a derivative of c_2 or provide a measured quantity that is only indirectly related to c_2. Thus they do not provide the absolute solute concentration at any position in the cell. Although only concentration ratios are needed for Equations 11-49 and 11-52, these ratios cannot be calculated unless the absolute concentration is known at some position for calibration.

One way to circumvent the problem of concentration determination is to perform the equilibrium ultracentrifugation at sufficiently high rotor speeds so that no solute is left at the meniscus. This technique (the Yphantis meniscus-depletion method) allows use of the meniscus as a reference point for the optical system.

When appropriate precautions are taken, rather accurate molecular weights can be obtained from equilibrium centrifugation; Table 11-2 gives some representative results, which show that among various methods compared, equilibrium centrifugation is the most consistently accurate.

Equilibrium ultracentrifugation of mixtures of macromolecules

Suppose that the solution is not homogeneous, but instead is a mixture with i components. In such cases, curved lines may be observed when $\ln c_2$ is plotted against x^2. If there are c_i g cm^{-3} of material with molecular weight M_i, then Equation 11-49

becomes

$$c_T(x) = \sum_i c_i(x) = \sum_i c_i(x_0) \exp[M_i(1 - \bar{V}_{2i}\rho)\omega^2(x^2 - x_0^2)/2RT \qquad (11\text{-}53)$$

where $\bar{V}_{2i}$ is the partial specific volume of the ith component, and c_T represents the total weight concentration of solute. In principle, it is possible to fit such a function and derive values of $M(1 - \bar{V}_2\rho)$ for each of the individual components. Very accurate data are required, and it is rare to have sufficient accuracy in practice to justify a fit to more than two components. Substances with close molecular weights can never be resolved accurately by such a fitting approach.

One alternative is to settle for average molecular weight data. If the partial specific volume is the same for each component, differentiation of Equation 11-53 yields

$$\begin{aligned} d[\ln c_T(x)]/dx^2 &= [(1 - \bar{V}_2\rho)\omega^2/2RT]\left[\sum_i M_i c_i(x) \Big/ \sum_i c_i(x)\right] \\ &\equiv [(1 - \bar{V}_2\rho)\omega^2/2RT]\bar{M}_w(x) \end{aligned} \qquad (11\text{-}54)$$

The average molecular weight $\bar{M}_w(x)$ given by Equation 11-54 is a weight average, because c_T and c_i are weight concentrations. (See Box 11-3.) Equation 11-54 allows us to determine the weight-average molecular weight $\bar{M}_w(x)$ at each point x in the cell. The value of $\bar{M}_w(x)$ should increase with x, because heavy molecules will tend to be located farther from the rotation axis at equilibrium.

Often what we desire is the average molecular weight of the entire sample. We could obtain this value by integrating Equation 11-54 from the meniscus to the cell bottom, but it is simpler to obtain it another way. Starting from Equation 11-52, for a mixture of components, we can write

$$\sum_i c_{ib} - \sum_i c_{im} = \sum_i c_{i0} M_i(1 - \bar{V}_2\rho)\omega^2(x_b^2 - x_m^2)/2RT \qquad (11\text{-}55)$$

where c_{ib} and c_{im} are the equilibrium concentrations of the ith component at the bottom and at the meniscus of the cell, respectively, and c_{i0} is the initial concentration of the ith component. Dividing both sides of this equation by $\sum_i c_{i0} = c_{T,0}$, and recognizing that the two sums in the left-hand side of the equation are just the total concentrations at the bottom and the meniscus at equilibrium, we obtain

$$[c_T(x_b) - c_T(x_m)]/c_{T,0} = [(1 - \bar{V}_2\rho)\omega^2/2RT](x_b^2 - x_m^2)\bar{M}_w \qquad (11\text{-}56)$$

where $\bar{M}_w$ clearly is the weight-average molecular weight of the entire mixture. (It often is called a cell-average $\bar{M}_w$.)

Other average molecular weights can be obtained if the data are treated differently. It is difficult to obtain the number-average molecular weight from centrifugation, but the z average at each cell position (see Box 11-3) can be calculated from observed data. It can be shown that

$$\begin{aligned} \bar{M}_z(x) &= \sum_i M_i^2 c_i \Big/ \sum_i M_i c_i \\ &= [2RT/(1 - \bar{V}_2\rho)\omega^2](d\{\ln [c_T(x)\bar{M}_w(x)]\}/dx^2) \end{aligned} \qquad (11\text{-}57)$$

Then the cell-average $\bar{M}_z$ is obtained by integrating from the meniscus to the cell bottom. Equations 11-54 and 11-57 provide a sensitive test of the homogeneity of a substance. A pure single component with no tendency to self-associate should have identical values of $\bar{M}_z(x)$ and $\bar{M}_w(x)$ at each position in the cell.

Ultracentrifugation of a monomer–dimer equilibrium system

Suppose one is dealing with an associating macromolecular system. The various components must be in equilibrium at every point in the centrifuge cell. If there is no change in the partial specific volume during the association, then the equilibrium constant will be the same as that for a sample unperturbed by centrifugation. However, the equilibrium will shift with pressure if there is a net change in molecular volumes. The pressures generated in an ultracentrifuge can be considerable. The pressure gradient will be $dP/dx = \rho\omega^2 x$; therefore, $P(x) = (P/2)\omega^2(x^2 - x_m^2)$. The pressure can amount to several hundred atmospheres at the bottom of the cell.

To keep things simple, consider the monomer–dimer equilibrium, $2\,P \rightleftharpoons P_2$, characterized by the equilibrium constant

$$\bar{k} = c_2/c_1^2 \qquad (11\text{-}58)$$

Pressure effects will be ignored, which means that $\bar{V}_2$ must be the same for all associating species. Because weight units are used, $\bar{k}$ differs from the usual equilibrium constant by a factor of $2/M_1$, where M_1 is the monomer molecular weight.

First, let us show that this equilibrium expression is obeyed at every position x in the cell. Suppose we have a mixture of a monomer and a dimer that are not equilibrating. The distribution of each separate species within the cell is given by Equation 11-49:

$$c_1(x) = c_1(x_0) \exp\{[M_1(1 - \bar{V}_2\rho)\omega^2/2RT](x^2 - x_0^2)\} \qquad (11\text{-}58a)$$

$$c_2(x) = c_2(x_0) \exp\{[2M_1(1 - \bar{V}_2\rho)\omega^2/2RT](x^2 - x_0^2)\} \qquad (11\text{-}58b)$$

Dividing these two equations yields

$$c_2(x)/c_1(x) = [c_2(x_0)/c_1(x_0)] \exp\{[M_1(1 - \bar{V}_2\rho)\omega^2/2RT](x^2 - x_0^2)\} \qquad (11\text{-}58c)$$

But the exponential term is simply $c_1(x)/c_1(x_0)$, so we have the following result:

$$c_2(x)/c_1^2(x) = c_2(x_0)/c_1^2(x_0) \qquad (11\text{-}58d)$$

This relationship is independent of the rotor speed ω, and it is the same at all positions in the cell. Thus, if we load a centrifuge cell with a monomer–dimer mixture at equilibrium, so that Equation 11-58 is obeyed initially, the equilibrium distribution will be preserved at any speed and at all positions in the cell.

In the ultracentrifuge, we cannot observe the monomer and dimer separately, but only the total weight concentration c_T as described by Equation 11-53. The

Box 11-3 MOLECULAR WEIGHT AVERAGES

Consider a sample containing a distribution of species with different molecular weights. Let $n(M)dM$ be the number of moles of species with molecular weight between M and $M + dM$. The total number n_T of moles of species in the sample is

$$n_T = \int_0^\infty dM n(M)$$

The function $n(M)$ is called a molecular weight distribution function. If it were known explicitly, it would provide a complete description of all species in the sample. Often, however, it is desirable or necessary to deal with a less precise description. For example, we can define moments of the distribution function $n(M)$. The kth moment of the function is

$$m_k = \int_0^\infty dM n(M) M^k$$

Thus, n_T is the zeroth moment; it is just the area under the function.

Average molecular weights are defined as the ratios of various higher (kth) moments of $n(M)$ to the $(k-1)$th moment. The number-average molecular weight is defined as

$$\bar{M}_n \equiv m_1/m_0 = \int_0^\infty dM n(M) M \Big/ \int_0^\infty dM n(M)$$

Consider a discrete distribution of species, containing n_i moles of components with molecular weight i. In this case, we can write the expression for $\bar{M}_n$ as

$$\bar{M}_n = \left(\sum_i n_i M_i\right) \Big/ \sum_i n_i$$

We can write $\bar{M}_n$ in terms of molar concentrations, simply by dividing both numerator and denominator of this expression by the volume V of the sample:

$$\bar{M}_n = \left[\left(\sum_i n_i M_i\right)\Big/V\right] \Big/ \left[\left(\sum_i n_i\right)\Big/V\right]$$

The weight concentration units used in hydrodynamics are g cm^{-3}, so $c_i = n_i M_i / V$. Thus, the number-average molecular weight can be written as

$$\bar{M}_n = \left(\sum_i c_i\right) \Big/ \sum_i (c_i/M_i)$$

The weight-average molecular weight is defined as the ratio of the second moment to the first moment of the distribution function:

$$\bar{M}_w \equiv m_2/m_1 = \left(\sum_i n_i M_i^2\right) \Big/ \sum_i n_i M_i$$

Substituting weight concentrations just as before, we can write

$$\bar{M}_w = \left(\sum_i c_i M_i\right) \Big/ \sum_i c_i$$

Because $\sum_i c_i$ is the total weight concentration of solute (c_T), each term in $\bar{M}_w$ is just equivalent to the weight fraction w_i with molecular weight M_i in the sample.

A third molecular weight average commonly used is the z-average molecular weight:

$$\bar{M}_z \equiv m_3/m_2 = \left(\sum_i n_i M_i^3\right) \Big/ \sum_i n_i M_i^2 = \left(\sum_i c_i M_i^2\right) \Big/ \sum_i c_i M_i$$

For a mixture of components with very different molecular weights, the values of $\bar{M}_n$, $\bar{M}_w$, and $\bar{M}_z$ are quite disparate. Consider a 1:1 weight mixture of two macromolecules, one with molecular weight 10^3, and the other of 10^5 mol wt. The resulting averages are

$$\bar{M}_n = (1+1)/[(1/10^3) + (1/10^5)] = 1{,}950$$

$$\bar{M}_w = [(1 \times 10^3) + (1 \times 10^5)]/(1+1) = 50{,}500$$

$$\bar{M}_z = \{[1 \times (10^3)^2] + [1 \times (10^5)^2]\}/[(1 \times 10^3) + (1 \times 10^5)] = 99{,}020$$

Different experimental techniques provide different average molecular weights. Thus, if two or more different average values were measured, it would be very easy to see that the sample being studied must be a mixture. Ultracentrifugation provides values for $\bar{M}_w$ and $\bar{M}_z$. Light scattering measures $\bar{M}_w$ (see Chapter 14). To measure $\bar{M}_n$ directly, one must use techniques such as osmotic-pressure or vapor-pressure measurements.

following is one approach for obtaining the equilibrium constant. The total weight concentration of a monomer–dimer equilibrium mixture is

$$c_T = c_1 + c_2 = c_1 + \tilde{k}c_1^2 \tag{11-59}$$

It is convenient to differentiate Equation 11-59:

$$dc_T/dc_1 = 1 + 2\tilde{k}c_1 \tag{11-60}$$

Because of the equilibrium reaction, the weight-average molecular weight at each position in the cell now is a function of c_T as well:

$$\bar{M}_w(c_T) = (M_1c_1 + 2M_1c_1^2\tilde{k})/c_T = [M_1c_1(1 + 2c_1\tilde{k})]/c_T \tag{11-61}$$

Inverting Equation 11-60, and using Equation 11-61 to replace the term $1 + 2c_1\tilde{k}$, we can write

$$dc_1/dc_T = 1/(1 + 2c_1\tilde{k}) = (c_1/c_T)[M_1/\bar{M}_w(c_T)] = w_1M_1/\bar{M}_w(c_T) \tag{11-62}$$

where we have defined $w_1 = c_1/c_T$ as the weight fraction of monomer. If we differentiate this definition of w_1, we obtain an alternative expression for dc_1/dc_T:

$$dc_1/dc_T = w_1 + c_T(dw_1/dc_T) \tag{11-63}$$

Setting Equation 11-62 equal to Equation 11-63, and rearranging, we obtain

$$d(\ln w_1)/d(\ln c_T) = [M_1/\bar{M}_w(c_T)] - 1 \tag{11-64}$$

Equation 11-64 can be integrated between two positions in the cell, x_0 and x, to give

$$\ln [w_1(x)/w_1(x_0)] = \int_{c_T(x_0)}^{c_T(x)} \{[M_1/\bar{M}_w(c_T)] - 1\}(dc_T/c_T) \tag{11-65}$$

To use this equation, we must have data that extend to such a low concentration that $c_T(x_0) \cong 0$. Then $w_1(x_0) = 1$. We can obtain $c_T(x)$ directly in an equilibrium ultracentrifugation experiment. Using Equation 11-54, we can obtain $\bar{M}_w(x)$, and hence we can calculate $\bar{M}_w(c_T)$. Thus, as long as M_1 is known independently, we can obtain $\ln w_1$ at each position in the cell by integrating a plot of $\{[M_1/\bar{M}_w(c_T)] - 1\}c_T^{-1}$ versus c_T. We then can compute the equilibrium constant as

$$\tilde{k} = (1 - w_1)/w_1^2c_T \tag{11-66}$$

More elaborate equilibria require more complex treatments, but the overall results are similar. Equilibrium ultracentrifugation is an excellent method for studying

macromolecular associations. In real cases, however, one must use equations more sophisticated than Equation 11-65—equations that take nonideality into account.

Analysis of the approach to equilibrium

Equilibrium ultracentrifugation is a very powerful technique, but it is a very time-consuming measurement. Even with short columns, a day or two is required for 500,000 d samples to reach equilibrium, and a few hours for 50,000 d samples. A popular alternative is to analyze low-speed sedimentation data of samples on the way to equilibrium. Such data are typified by the intermediate time point in Figure 11-18. In 1947, W. J. Archibald (who had been working for years on solutions of the Lamm equation) realized that, at the meniscus or at the bottom of the cell, the flux equation can be solved trivially at all times in a sedimentation experiment. The flux J_2 must be zero at the meniscus and at the bottom of the cell, because no material can pass through these points. This fact is uninteresting at high rotor speeds, because there is no solute at the meniscus, and a pellet is formed at the bottom. However, at low speeds, Equation 11-4 set equal to zero immediately yields

$$\omega^2 s/D = (\partial c_2/\partial x)(1/xc_2) \qquad \text{for } x = x_b \text{ or } x_m \text{ only} \tag{11-67}$$

Substituting expressions for s and D, we can write

$$M_m = [RT/(1 - \bar{V}_2\rho)\omega^2](\partial c_2/\partial x)_{x_m}(1/x_mc_m) \tag{11-68a}$$

$$M_b = [RT/(1 - \bar{V}_2\rho)\omega^2](\partial c_2/\partial x)_{x_b}(1/x_bc_b) \tag{11-68b}$$

where c_m and c_b are the concentrations at the meniscus and at the bottom, respectively. With these expressions, we can obtain two estimates of the molecular weight at any time if we can measure the solute concentration and its gradient at top and at bottom. For a homogeneous sample, the two molecular weights should be equal. The Archibald method thus provides a good test of homogeneity.

The difficulty in using Equation 11-68 lies in measuring both the concentrations and their gradients. If absorption optics are used, the concentrations are obtained, and these must be numerically differentiated to obtain gradients. Such a procedure magnifies the noise in a concentration-versus-distance plot, resulting in imprecision. Schlieren optics help, because they give gradients directly. A plateau region remaining in the cell makes it easier to extract the concentrations at the bottom and at the meniscus from Schlieren data. One can always write

$$c_m = c_p - \int_{x_m}^{x_p} (\partial c/\partial x)\,dx \tag{11-69a}$$

$$c_b = c_p + \int_{x_p}^{x_b} (\partial c/\partial x)\,dx \tag{11-69b}$$

By considering the total material between x_m and x_p, or between x_p and x_b, and conserving mass, one can show that

$$c_m = c_0 - (1/x_m^2)\int_{x_m}^{x_p} x^2(\partial c/\partial x)\,dx \qquad (11\text{-}70a)$$

$$c_b = c_0 + (1/x_b^2)\int_{x_p}^{x_b} x^2(\partial c/\partial x)\,dx \qquad (11\text{-}70b)$$

where c_0 is the initial uniform concentration of solute. If no plateau exists, more complex approaches can be used (see Schachman, 1959). Any of these transient-state methods rapidly provide a value for the molecular weight.

Density-gradient ultracentrifugation: simple theory

Suppose a concentrated solution of a small molecule is spun at high speeds in the ultracentrifuge until equilibrium is reached. According to Equation 11-49, the small solute (component 3) will redistribute in the cell in just the same way as a large molecule might. If we use the meniscus of the cell as a reference point, and we expand the exponential in Equation 11-49 because M is small, we obtain

$$c_3(x)/c_3(x_m) = 1 + [M_3(1 - \bar{V}_3\rho)\omega^2/2RT](x^2 - x_m^2) \qquad (11\text{-}71)$$

This expression is only approximate, because ρ is a function of x for a concentrated solution, and nonideality effects cannot be neglected. So Equation 11-49 is not exact to begin with. But, ignoring these complications for the moment, one can see that a parabolic concentration distribution is predicted. The density of the solution is roughly linear in the concentration of solute. This means that an equilibrium density gradient is established. From Equation 11-71, we have $\partial\rho/\partial x \propto \partial c_3/\partial x \propto \omega^2 x$. In practice, using salts of heavy metals such as CsCl, one can create a gradient of more than 10% in density across a typical centrifuge tube at the top speeds of modern ultracentrifuges.

Now consider the effect of adding a small amount of a macromolecule to the salt solution prior to centrifugation. If the macromolecule (component 2) is more dense than the highest density of CsCl at the bottom of the gradient, it will pellet to the bottom. If it is less dense than the lowest CsCl density, it will float to the top. However, if the macromolecular density falls within the range of the gradient, it will collect in a band at the density where $(1 - \bar{V}_2\rho)$ is zero (Fig. 11-19). If the density gradient is known, then the density (and thus $\bar{V}_2$) of the macromolecule can be determined from its position in the cell. At the center of the band, $\bar{V}_2^{-1}$ is just equal to the solution density ρ_0 at that point. This density is called the buoyant density. A mixture of macromolecules with different densities can be separated preparatively

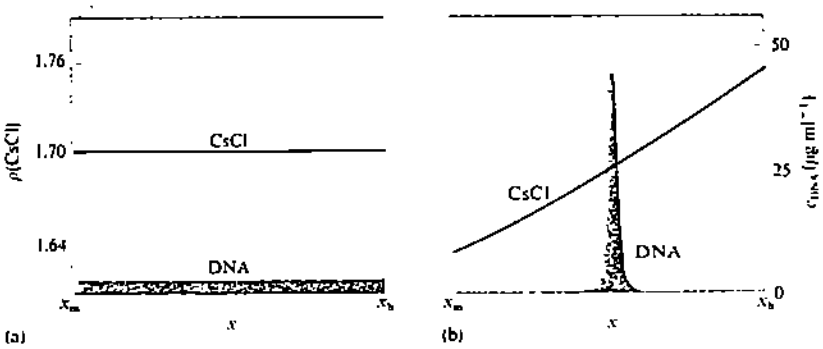

Figure 11-19

Equilibrium ultracentrifugation of a small amount of DNA in a CsCl gradient. (a) The density distribution at the beginning of the experiment. (b) The density distribution at equilibrium. [After W. Szybalski, *Fractions* (Beckman Instruments, Inc., 1968), no. 1, p. 1.]

by such centrifugation. The resolution is potentially very sharp, because (in principle) the density gradient can be made quite shallow. Thus, it is important to examine the factors that determine the width of the band of a macromolecule.

Still ignoring three-component thermodynamic effects, consider just a pure physical density gradient. In the region of the macromolecule, we can expand the density in a Taylor series:

$$\rho(x) = \rho_0 + (x - x_0)(d\rho/dx)_{x_0} \qquad (11\text{-}72)$$

where x_0 is the center of the equilibrium band position of the macromolecule. Substitute this expression into Equation 11-48, the equilibrium distribution of the macromolecule. Neglecting nonideality, we obtain

$$M_2(1 - \bar{V}_2)\{[\rho_0 + (x - x_0)(d\rho/dx)_{x_0}]\}x = (RT/\omega^2)(1/c_2)(dc_2/dx) \qquad (11\text{-}73)$$

This equation is simplified by recognizing that $\bar{V}_2\rho_0 = 1$, as we have mentioned earlier. Then letting $y = x - x_0$, and $dy = dx$, we can rewrite Equation 11-73 as

$$d(\ln c_2) = (-M_2\omega^2/RT)\{(d\rho/dx)_{x_0}\bar{V}_2(y^2 + x_0 y)\,dy \qquad (11\text{-}74)$$

Because y is much smaller than x_0, the term in y^2 can be dropped. Integrating from $y = 0$ to $y = x$, and replacing y with $x - x_0$, we obtain

$$c_2(x) = c_2(x_0)\exp[-(x - x_0)^2/2\sigma^2] \tag{11-75}$$

Thus, a macromolecule in a density gradient distributes in a Gaussian band with a width characterized by standard deviation σ, which is given by

$$\sigma^2 = RT/M_2\bar{V}_2\omega^2 x_0(d\rho/dx)_{x_0} \tag{11-76}$$

Density-gradient centrifugation: three-component theory

To solve the density-gradient equilibrium problem correctly, one must explicitly consider the thermodynamics of all three components. The molar concentration of macromolecule within the band is high enough that it cannot be neglected. Preferential interaction between components 2 and 3 can alter the density gradient, the shape of the band, and the apparent buoyant density (ρ_0). It is quite a complicated problem, and we sketch here only a few features.

We start with the general phenomenological equation for the flux of the ith component in a three-component system (see Eqn. 10-38):

$$J_i = \sum_{j=1}^{3} L_{ij}X_j \tag{11-77}$$

where X_j is the generalized force on component j. In the ultracentrifuge, we know (by comparing Eqns. 11-77 and 11-29) that the force on the jth component is

$$X_j = \omega^2 x - \partial\tilde{\mu}_j/\partial x \tag{11-78}$$

At mechanical and thermal equilibrium, this force must be zero. Hence,

$$\omega^2 x = \partial\tilde{\mu}_j/\partial x \tag{11-79a}$$

The gradient of the chemical potential of component j can be evaluated in the same way as that shown earlier for a two-component system (Eqns. 11-30 and 11-31). The result allows Equation 11-79a to be rewritten as

$$(1 - \bar{V}_j\rho)\omega^2 x = \sum_{i=1}^{3} (\partial\tilde{\mu}_j/\partial c_i)(\partial c_i/\partial x) \tag{11-79b}$$

In density-gradient centrifugation, the third component is the concentration of a heavy salt such as CsCl. We first seek a description of the density gradient generated by this component. This gradient can arise from concentration effects and pressure effects:

$$d\rho/dx = (\partial\rho_C/\partial x) + (\partial\rho_P/\partial x) \tag{11-80}$$

One starts by making the approximation that the chemical potential of component 3 is independent of the concentrations of components 1 and 2. Then,

$$(1 - \bar{V}_3\rho)\omega^2 x = (\partial\tilde{\mu}_3/\partial c_3)_\rho(\partial c_3/\partial x) \tag{11-81}$$

Using Equation 11-81, we can write the density gradient due to the composition of component 3 (low-molecular-weight solute such as salt) as

$$\partial\rho_C/\partial x = (\partial\rho/\partial\tilde{\mu}_3)(\partial\tilde{\mu}_3/\partial c_3)(\partial c_3/\partial x) = g\omega^2 x \tag{11-82}$$

where the constant $g = (1 - \bar{V}_3\rho)(\partial\rho/\partial\tilde{\mu}_3)$. The derivative $\partial\rho/\partial\tilde{\mu}_3$ can be measured from the dependence of density on the activity of component 3. There is also a compression density gradient:

$$\partial\rho_P/\partial x = (\partial\rho/\partial P)(\partial P/\partial x) = k\omega^2 x \tag{11-83}$$

where $k = \partial\rho/\partial P$ is another constant. The overall density gradient is the sum of these two effects (from Eqn. 11-80):

$$d\rho/dx = (k + g)\omega^2 x \tag{11-84}$$

Next we calculate the position of the macromolecule band. In a three-component system, the third component need not be included explicitly, because there are only two independent chemical potential variables in a three-component system (see also Box 10-1). It is convenient to ignore the salt and to work only with solvent and macromolecule. Now, however, components 1 (water) and 2 (macromolecule) must be treated by two-component thermodynamics. Equation 11-79b becomes

$$(1 - \bar{V}_1\rho)\omega^2 x = (\partial\tilde{\mu}_1/\partial c_1)_{c_2}(\partial c_1/\partial x) + (\partial\tilde{\mu}_1/\partial c_2)_{c_1}(\partial c_2/\partial x) \tag{11-85a}$$

$$(1 - \bar{V}_2\rho)\omega^2 x = (\partial\tilde{\mu}_2/\partial c_2)_{c_1}(\partial c_2/\partial x) + (\partial\tilde{\mu}_2/\partial c_1)_{c_2}(\partial c_1/\partial x) \tag{11-85b}$$

where the concentration of component 2 is now explicitly allowed to affect the chemical potential of component 1, and vice versa.

The difficulty in solving Equation 11-85 arises from the two-component effects: $(\partial\tilde{\mu}_1/\partial c_2)_{c_1}$ and $(\partial\tilde{\mu}_1/\partial c_1)_{c_2}$. However, because the chemical potential of component 1 is a function of both components, a change in this potential resulting from a change in solution can be described as

$$d\tilde{\mu}_1 = (\partial\tilde{\mu}_1/\partial c_1)_{c_2}\,dc_1 + (\partial\tilde{\mu}_1/\partial c_2)_{c_1}\,dc_2 \tag{11-86}$$

If the change $d\tilde{\mu}_1$ is carried out by varying component 1 at constant $\tilde{\mu}_1$, the result is

$$0 = (\partial\tilde{\mu}_1/\partial c_1)_{c_2}(\partial c_1/\partial c_1)_{\tilde{\mu}_1} + (\partial\tilde{\mu}_1/\partial c_2)_{c_1}(\partial c_2/\partial c_1)_{\tilde{\mu}_1} \tag{11-87}$$

By rearranging this, we can define a solvation parameter as

$$\Gamma' = (\partial c_1/\partial c_2)_{\tilde{\mu}_1} = -(\partial\tilde{\mu}_1/\partial c_2)_{c_1}/(\partial\tilde{\mu}_1/\partial c_1)_{c_2} \tag{11-88}$$

This parameter is essentially the weight of solvent that also must be added when adding a gram of macromolecule in dilute solution to keep the chemical potential of solvent constant. It is, therefore, a measure of the amount of bound solvent.

The parameter Γ' is the three-component equivalent of the gram/gram hydration parameter we used previously. Using Equation 11-88, we can solve Equation 11-85 as follows. First, note that $(\partial\tilde{\mu}_2/\partial c_1) = (\partial\tilde{\mu}_1/\partial c_2)$, because both are equal to $\partial^2 G/\partial c_1\partial c_2$, where G is the Gibbs free energy. We can use $-\Gamma'\partial\tilde{\mu}_1/\partial c_1$ to replace $\partial\tilde{\mu}_1/\partial c_2$. Then Equations 11-85a and 11-85b can be solved simultaneously to eliminate the unknowns $(\partial\tilde{\mu}_1/\partial c_1)_{c_2}$ and $\partial c_1/\partial x$. After considerable tedious manipulation, the resulting equation can be arranged in the form of Equation 11-81:

$$(1 + \Gamma')\{1 - [(\bar{V}_2 + \Gamma'\bar{V}_1)/(1 + \Gamma')]\rho\}\omega^2 x = (\partial\tilde{\mu}_2/\partial c_2)_{c_1}(\partial c_2/\partial x) \tag{11-89}$$

In a density-gradient equilibrium, the buoyant density (ρ_0) is operationally the point at which the macromolecule concentration is at a maximum. Thus $\partial c_2/\partial x = 0$, and

$$1/\rho_0 = (\bar{V}_2 + \Gamma'\bar{V}_1)/(1 + \Gamma') \equiv \bar{V}_s \tag{11-90}$$

where we define a solvated partial specific volume $\bar{V}_s$ as the inverse of the buoyant density.

Equation 11-89 can be put in a more familiar form by recalling that

$$(\partial\tilde{\mu}_2/\partial c_2)_{c_1} = (RT/M_2)[\partial(\ln a_2)/\partial c_2] = (RT/M_2 c_2)\{1 + [\partial(\ln\gamma_2)/\partial(\ln c_2)]\} \tag{11-91}$$

Thus we can write

$$M_2(1 + \Gamma')(1 - \bar{V}_s\rho)\omega^2 x/\{1 + [\partial(\ln\gamma_2)/\partial(\ln c_2)]\} = (RT/c_2)(\partial c_2/\partial x) \tag{11-92}$$

Comparison of Equations 11-92 and 11-48 shows that the apparent molecular weight that enters into Equation 11-92 is a solvated molecular weight: $M_s = M_2(1 + \Gamma')$.

The solvated quantities $\bar{V}_s$ and M_s vary with density because the concentration of solvent (and thus the solvation) changes with position in the gradient. Thus the effective density gradient, $(\partial\rho/\partial x)^{\text{eff}}$, must be the physical gradient (Eqn. 11-84) corrected for this effect. It is reasonable that the macromolecule perturbs the gradient by interacting with solvent. When all of these factors are taken into account (including the nonideality of the macromolecular solution), an equation can be derived that has the same Gaussian form as Equation 11-75, with a width of

$$\sigma^2 = RT/M_z^{\text{app}}(x_0)\bar{V}_s(x_0)(\partial\rho/\partial x)^{\text{eff}}_{x_0}\omega^2 x_0 \tag{11-93}$$

where the apparent solvated molecular weight (M_z^{app}) is related to the true solvated weight (M_s) by a virial expansion:

$$M_z^{\text{app}} = M_s[1 + 2B_2 c_2(x_0) + \cdots]^{-1} \tag{11-94}$$

where B_2 is a constant.

It must be apparent that the use of Equations 11-90 and 11-93 to obtain absolute molecular weights and densities is a formidable problem. The usual practice is to use Equation 11-84 to approximate $(\partial\rho/\partial x)^{\text{eff}}$, because all the quantities in this equation are measurable. A macromolecule with known or assumed ρ_0 is placed in the gradient, and unknowns are compared to the standard by their relative positions in the gradient. For more accurate work, $(\partial\rho/\partial x)^{\text{eff}}$ can be determined by using isotopically substituted samples, such as [^{15}N]-DNA versus [^{14}N]-DNA. In this case, it can be assumed that the isotopic substitution changes none of the thermodynamic parameters, but alters only the anhydrous molecular weight and density of the macromolecule. Once $(\partial\rho/\partial x)^{\text{eff}}$ is known, then Equation 11-93 will yield an accurate molecular weight from the shape of the band.

Note that the considerations leading to Equation 11-92 should apply to any three-component system, whether or not the third component has a substantial effect on the density of the solution. This sensitivity to other components might appear to introduce serious complications into any ultracentrifugation experiment. Fortunately, methods have been developed to circumvent such complications (see Box 11-4).

Equilibrium density-gradient sedimentation occasionally has been applied to proteins, but most work involves nucleic acids. Chapter 22 gives examples of results from this technique.

Box 11-4 ULTRACENTRIFUGATION IN THREE-COMPONENT SYSTEMS

E. F. Casassa and H. Eisenberg have developed a useful technique for determining the molecular weight of a solute in a three-component system, unaffected by three-component effects such as preferential solvation. Here we only sketch the results; for a detailed treatment, see H. Fujita (1975).

Casassa and Eisenberg showed that, in the limit of low macromolecule concentration ($c_2 \to 0$), it is possible to evaluate the terms in the left-hand side of Equation 11-89 as

$$(1 + \Gamma')\{1 - [(\bar{V}_2 + \Gamma'\bar{V}_1)/(1 + \Gamma')]\rho\} = (\partial\rho/\partial c_2)_{\tilde{\mu}_1,\tilde{\mu}_3}$$

Experimentally, this evaluation is accomplished by dialyzing a solution of macromolecule and salt against a large volume of salt solution, and measuring the density of the macromolecule solution after equilibrium is reached. Then the results of an equilibrium ultracentrifugation experiment can be evaluated from Equation 11-92 (with nonideality terms deleted because $c_2 \to 0$) as

$$d(\ln c_2)/d(x^2) = (M_2\omega^2/2RT)(\partial\rho/\partial c_2)_{\tilde{\mu}_1,\tilde{\mu}_3}$$

Similarly, velocity sedimentation experiments can be analyzed by replacing $1 - \bar{V}_2\rho$ in Equation 11-28 with the three-component equivalent, $(\partial\rho/\partial c_2)_{\tilde{\mu}_1,\tilde{\mu}_3}$.

Summary

Sedimentation velocity experiments measure the rate at which a macromolecule moves when subjected to radial acceleration in an ultracentrifuge. The rate per unit field, s, is proportional to the molecular weight and inversely proportional to the frictional coefficient. Thus, for spherical particles, $s \propto M^{2/3}$. In the ultracentrifuge, each pure component normally gives rise to a boundary. Above the boundary, the component is absent; beneath the boundary, in the plateau region, the concentration of the component is constant with distance, but varies with time. One can measure s by examining either the boundary or the plateau. The shape of the boundary is affected by diffusion but, in practice, the concentration dependence of s also has a strong influence on boundary shape. Very complex effects on boundary shape and height can result when several different macromolecular species are present. These effects can be circumvented by zonal centrifugation, in which one starts with a thin band of macromolecule-containing solution layered on top of a supporting solvent, rather than with a homogeneous sample. Stabilizing gradients allow recovery of physically separated samples after the solution is removed from the centrifuge.

At rotor speeds much smaller than those used for sedimentation velocity experiments, an equilibrium distribution of macromolecules is created in the ultracentrifuge. The shape of this distribution is proportional to the molecular weight, and it does not depend on frictional properties. When mixtures of components are present, equilibrium centrifugation yields a weight-average molecular weight. In some cases, the equilibrium distribution of associating macromolecules can be analyzed to yield the association constant. Density-gradient equilibrium ultracentrifugation is a powerful technique for separating macromolecules according to their buoyant densities. Here the macromolecule is allowed to equilibrate in a gradient of a heavy salt (such as CsCl) that spans its density. The macromolecule at equilibrium is found in a narrow band centered about its buoyant density. This buoyant density is not equal to the density of pure macromolecule because of complex three-component thermodynamic effects present in the concentrated salt solutions used to create the gradient. The width of the band of macromolecule is inversely proportional to the square root of the molecular weight.

Problems

11-1. Estimate the velocity (cm sec^{-1}) with which a 1 g copper sphere (a) will sink in a lake; (b) will move in aqueous solution in a centrifuge spinning at 1 rpm, 10 cm from the rotation axis.

11-2. Suppose you wish to measure the sedimentation constant of a substance present in small amounts contaminated by many impurities. You obviously cannot detect this substance in a meaningful way by optical methods in the ultracentrifuge. However, you can assay it in some biochemical way, such as "rats killed per cm^3 of solution." You make use of a separation cell (Fig. 11-20), initially filled with a solution at concentration c_0 as determined

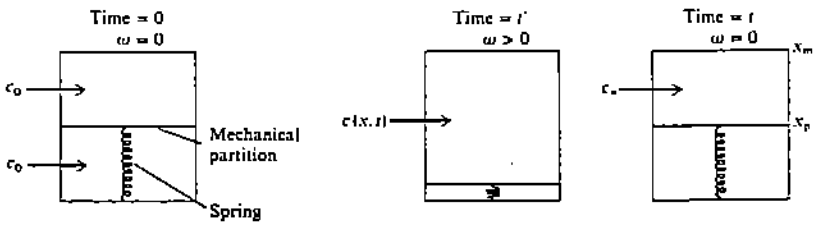

Figure 11-20
Separation-cell experiment for Problem 11-2.